BABEȘ-BOLYAI UNIVERSITY

Faculty of Physics

Doctoral School of Physics

DOCTORAL THESIS ABSTRACT

Advanced methods for characterizing biological materials

Ramona CRAINIC

Scientific Supervisor

Prof. Dr. Radu FECHETE

Cluj-Napoca

2025

Content

INTRODUCTION

Modern tissue engineering (tissue production engineering) uses regenerative cell treatments and advanced biomaterials to promote the recovery of tissues around a specific portion that has a malformation and is thus, targeted for recovery or regeneration. In this regard, electrospun nanofibers are widely applied in multiple biomedical applications, structures that support tissue development and regeneration in tissue engineering processes, in wound healing, drug administration, filtration, as an affinity membrane in very specific separation and purification processes, in enzyme immobilization, in small-diameter vascular graft implants, biotechnology, environmental engineering, energy storage and generation, and various other researches. The unique properties of these nanofibers, but also the low production costs, are an advantage, and the nanofibers obtained from electrospinning are becoming an important resource in research and industry, offering innovative alternatives for the future. Biosolids play a significant role in reducing pollution and restoring degraded land.

The major objective of the doctoral thesis is to develop a multivalent protocol used for the complex characterization, using advanced methods, of different types of biomaterials. This protocol involves multiple stages starting with i) the design and construction of an electrospinning device for the production of samples; ii) the local production (within the Applied Physics laboratory of the Department of Physics and Chemistry of the Technical University of Cluj-Napoca) of new materials such as nanofiber films (bio and non-bio) and fertilizers (in cooperation with the National Institute for Research and Development for Machines and Technology Installations for Agriculture and Food Industry-INMA Bucharest- Cluj-Napoca Branch); iii) choosing the most appropriate methods and techniques for characterizing biomaterials such as Nuclear Magnetic Resonance (with relaxometry techniques in low fields and spectroscopy of ^{1}H and ^{13}C in high fields); iv) complex characterization of nanofiber foil samples and organo-mineral fertilizers obtained within the experimental program of the doctoral thesis; v) application of a primary level of analysis of measured data such as 1D Fourier transform and 1D and 2D Laplace transform; vi) applying a secondary level of analysis such as the procedures for deconvolution and quantification of the content of the component elements; vii) statistical analysis in principal components to determine the most relevant parameters and correlations, used for the classification of samples, and viii) the use of modern techniques involving the use of artificial intelligence, in particular the use of artificial neural networks and machine learning tools for predicting the properties of biomaterials.

CHAPTER 1 Biological materials

1.1 Biomaterials obtained by electrospinning

Biomaterials are natural or synthetic materials specially designed to interact with biological systems. The most common approach to classifying biomaterials is based on the type of materials used. Thus, they can be classified into: metals, ceramics, polymers and composite substances. Also, depending on their source, they can be classified as natural or synthetic. An essential attribute of a biomaterial is biocompatibility. Thus, biocompatibility of biomaterials refers to the performance of any material placed in a specific biological environment to obtain an adequate response from the host [1]. Biomaterials are materials that have been used more and more often in medical science in recent decades. In the human body, a number of body tissues such as teeth, ligaments, bone tendons, and others have been successfully replaced by these biomaterials. At the moment, more and more diverse applications of biomaterials are predicted and expected to be put into practice, so they are to be studied more and more. An important challenge in the use of these biomaterials is the attenuation of immune rejection. Thus, the current standards of implants made for the whole life and bone replacement imply total biocompatibility of the biomaterial used with respect to the biological and mechanical characteristics of the replaced tissue. So far, a significant number of biomaterials have been discovered which, due to their biocompatibility and biodegradability, are frequently used in biotherapy and medical science. These biomaterials can be grouped into two categories, namely natural or synthetic polymers, which have thus gained quite a lot of attention [2].

1.1.1 Principles of fiber production by electrospinning

The electrospinning process is a widely used technology for the production of electrostatic fiber, which uses electrical forces to produce polymer fibers with diameters ranging from 2 nm to a few micrometers using polymer solutions from both natural and synthetic polymers [3]. This electrospinning process is an ancient technique, which was first observed in 1897 by Rayleigh and studied in detail by Zeleny in 1914 [4]. Taylor's 1969 work on electrically powered aircraft laid the groundwork for electrospinning [5]. Electrospinning is a spinning technique that uses electrostatic forces to produce fine fibers made from polymer solutions. To produce these fibers, an electrical voltage (kV) is required to generate electrospinning [6]. An electrospinning system consists of 3 major components (see Figure 1.1): a high-voltage source, syringe, and a grounded collection plate (or a rotating drum) that uses a high-voltage source to transmit the charge with a certain polarity in the polymer solution that is accelerated to a collector having opposite electrical polarity.

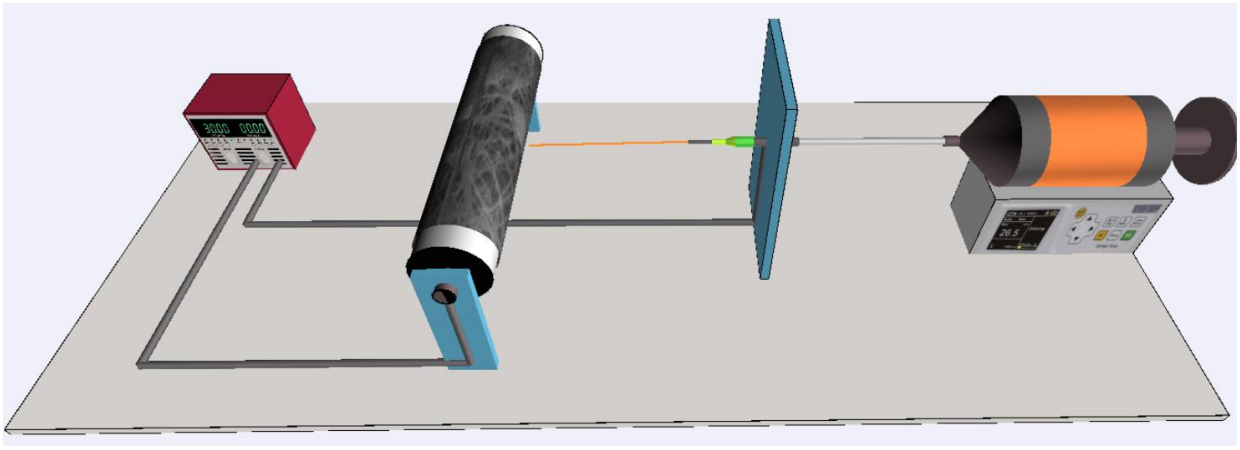

Fig. 1.1. Schematic diagram of an electrospinning device consisting of a syringe (tank of the electrospinning solution), driven by an injectomat (pump), a flexible tube leading to a metal needle fixed on a support, a drum (covered or made of an electrically conductive material) that rotates at variable speed by being driven by a motor and an adjustable high-voltage source with the positive terminal connected to the metal needle and the terminal connected to the spinning reel (a simulation of the electrospinning process can be watched at https://nmr4.utcluj.ro/Ramo/Electrospinning/).

Most polymers are dissolved with solvents before the electrospinning process. The polymer fluid is then fed into the syringe for electrospinning. Since the solvent or polymer used can emit unpleasant or even harmful odors, it is recommended that these processes be done in rooms with a ventilation system [7]. Thanks to the applied electric field, the Taylor Cone is formed, an electrically charged jet of solution that is thrown from the tip of the needle. During this process, the solvent evaporates and the polymer ends up on the collection plate in the form of fiber [8]. Thus, the electrospinning process offers a simplified technique for forming fibers.

1.1.2 Applications of fibers produced by electrospinning

More recently, various applications of fibers produced by electrospinning have begun to be analyzed. Electrospun nanofibers are widely applied in biomedical applications, structures that support tissue development and regeneration in tissue engineering processes (tissue production engineering), in wound healing, drug administration, filtration, as an affinity membrane in very specific separation and purification processes, in enzyme immobilization, in small-diameter vascular graft implants, biotechnology, in environmental engineering, in energy storage and generation but also in various other researches that are ongoing [9-11]. Electrospinning is a widely used production platform for tissue engineering, where, structures that closely mimic the extracellular matrix can be produced. Tissue engineering uses regenerative cellular treatments (scaffold-free methods) and advanced biomaterials (scaffold-based methods) to promote the recovery of tissues around a specific defective (injury) portion that is targeted for recovery/regeneration [12].

1.2 Biosolids

Biosolids are organic solids obtained by treating sludge obtained from wastewater treatment and treatment plants. During wastewater treatment, liquids are separated from solids, and the resulting solids may contain organic matter and nutrients. If these solids were to be used to obtain high-performance organo-mineral fertilizers, then, due to the low nutrient content of these biosolids, it is necessary to add fertilizers and mineral compounds to the production recipe. Their processing involves thermo-mechanical actions and reactive extrusion, which, through efficient mixing at the molecular level, facilitates the development of chemical reactions between components. Thus, a homogeneous structure, both physically and chemically, of the granules is obtained [13, 14]. Biosolids used in agriculture are organic solids obtained by digesting and stabilizing sludge resulting from wastewater treatment to reduce concentrations of pathogens and toxic chemicals below set levels, thus being able to be safely used as fertilizers without affecting the health of plants, soil and groundwater, and thus, indirectly, without affecting the health of consumers of agricultural or animal products [15-17]. Due to global population growth, urbanization and industrialization, the volume of wastewater and, as a result, the amount of raw sewage sludge and therefore biosolids is continuously increasing. On the other hand, population growth will lead to an increase in the demand for agricultural and food production. The degree to which this demand is met depends mainly on the amount of fertilizer used by farmers on their farmland. In these circumstances, the use of biosolids as fertilizer seems to be a very good option [18].

1.2.1 The main components of a biosolid used as a fertilizer

Typically, biosolids contain high concentrations of nitrogen (N), phosphorus (P), potassium (K), and sulfur (S) and several micronutrients, including copper (Cu), zinc (Zn), calcium (Ca), magnesium, boron (B), molybdenum (Mo), and manganese (Mn). For example, in Australia the rate of application of biosolids is determined by total nitrogen and the so-called NLBAR. However, one concern with NLBAR is the typically low N:P (nitrogen/phosphorus) ratio in biosolids. For example, with regard to fertilizer requirements for agricultural crops, it is intended that the application of N-based biosolids does not lead to an excess of P. When biosolids are applied routinely, this can lead to the progressive accumulation of soil P levels, increasing the risk of phosphorus transport to watercourses through erosion and runoff [19, 20].

The organo-mineral fertilizers based on biosolids studied within the experimental program were produced locally by INMA Bucharest – Cluj-Napoca Branch (National Institute for Research and Development for Machinery and Installations Designed for Agriculture and Food Industry).

In the recipes used, some components only have a fertilizer role and others, which are essential for ensuring the matrix and which makes reactive extrusion processing possible, also have a fertilizer role. The biosolid resulting from the composting of sludge from wastewater is an essential component that provides organic matter and partly macro and micro-nutrients. The biosolid used in the recipe was purchased from SEdC Mioveni, Romania. The organic matter content (around 43%) is about double the organic carbon content. This percentage of organic matter, due to its initial structure or due to the application of large amounts of mineral fertilizers, is very important for the regeneration of soils, especially those poor in this organic matter [21-23].

For the samples characterized in the present study, approximately 50 % of the solid fraction of the biosolid is organic matter and has a significant positive effect on the physical, chemical and biological properties of agricultural soil [17, 21]. Among others (see Table 1.1), the components introduced in the three versions of the formula (V1, V2 and V3) in relatively large quantities were: starch, protein hydrolysate and molasses. The commercial corn starch was obtained from SC Roquette SA Calafat and had a moisture content of 12.01 % and a density of 0.561 g/cm^3. The protein hydrolysate was obtained at the Cluj-Napoca Branch of INMA Bucharest.

Table 1.1. The composition of the manufacturing variants (V1, V2 and V3) of organo-mineral fertilizers based on biosolids [21].

Crt. No.	Raw material	V1 variant [%]	V2 variant [%]	V3 variant [%]
1	Dry biosolid (max. moisture 20%)	30.00	30.00	30.00
2	Dry biosolid (max. moisture 20%)	24.50	0.00	25.00
3	Mineral fertilizers (P/N 20:20)	0.00	24.00	0.00
4	Potassium nitrate (KNO_3)	22.20	23.10	23.00
5	Starch	7.98	7.47	7.50
6	Urea	5.30	6.30	6.20
7	Hydrolyzed protein (11 % solution)	4.00	4.00	4.00
8	Magnesium sulphate ($MgSO_4$)	3.30	2.82	3.56
9	Sugar beet molasses	2.23	1.89	0.00
10	Manganese sulphate ($MnSO_4$)	0.22	0.19	0.24
11	Iron sulphate ($FeSO_4$)	0.11	0.09	0.11
12	Zinc Sulphate ($ZnSO_4$)	0.08	0.07	0.09
13	Copper sulfate ($CuSO_4$)	0.05	0.04	0.06
14	Cobalt sulphate ($CoSO_4$)	0.03	0.03	0.03
15	Orthophosphoric acid (H_2PO_4)	0.00	0.00	0.21

1.2.2 Production of organo-mineral fertilizers based on biosolids

According to European Union regulations, organo-mineral fertilizer is defined as fertilizer obtained by mixing, chemical reaction, granulation or dissolving in water inorganic fertilizers having a declared content of one or more primary nutrients with organic fertilizers, or soil improver

[18]. The low nutrient content of biosolids means that for the production of high-performance organo-mineral fertilizers it is necessary to introduce mineral compounds into their manufacturing formula, in addition to biosolids, [17, 24]. The use of organo-mineral fertilizers in agriculture is increasing largely due to advantages over the single application of mineral fertilizers or organic additives [25]. The combination of organic and mineral fertilizers improves the interaction between minerals and plants by reducing the mineral absorption of phosphorus, increasing the availability of phosphorus from plants, increasing the biological activity of the soil and activating the activity of the roots of young plants [26-28]. Among the different physical forms of presentation of organo-mineral fertilizers, the most suitable is the granular one. Granular organo-mineral fertilizers have a low content of water and other volatile substances, require less storage space, pollute the environment less by eliminating the possibility of dust formation, allow the mechanization of application on the soil and thus the precision of spreading [29].

The process of producing organo-mineral fertilizer based on granular biosolid involves several stages. The first step is the preparation of the raw materials which consists of grouping and mixing them into two categories: i) a mixture of solid components (dry biosolid, mono-ammonium phosphate or mineral fertilizer N/P 20:20, potassium nitrate and starch) and ii) a mixture of liquid components (protein hydrolysate in which urea, molasses and microelements in the form of sulphate are dissolved) [13].

Fig. 1.2. a) Device for the production of organo-mineral fertilizers based on biosolids located at INMA Bucharest Cluj-Napoca Branch and b) organo-mineral fertilizers based on biosolids (V1, V2, V3) produced by INMA Bucharest Cluj-Napoca Branch [13, 14].

CHAPTER 2 ADVANCED METHODS OF CHARACTERIZATION OF BIOMATERIALS

2.1 Nuclear magnetic resonance

2.1.1 Principles of nuclear magnetic resonance

Nuclear Magnetic Resonance (NMR) is an extremely powerful technique for the analysis of materials of various types. There is no other method that can boast such great applicability in so many fields, such as: the study of organic and inorganic chemistry, polymers, catalysts and membranes, materials such as ceramics, cement, bottles and zeolites, superconductors, paints and wood, as well as biomaterials – including the brain, soft and hard tissues, cells, proteins, blood and plasma. This field of investigation also covers food, plant and soil processing, geology, oil exploration and even the study of Antarctic ice.

2.1.2 Bloch equations and spin-lattice relaxation times, T_1 and spin-spin, T_2

In Nuclear Magnetic Resonance, the evolution of nuclear magnetization $\vec{M}(t)$ under the influence of an external magnetic field $\vec{B}_0(t)$ is represented, in an empirical manner, by the Bloch equations. Thus, it can be considered that macroscopic nuclear magnetization (for a statistically, relevant set of spines) is the source of the NMR signal, S(t), from which the information is collected by specific analyses. If we assume that the investigated system is considered as a "black box" characterized by transverse (T_2) and longitudinal (T_1) relaxation times, equilibrium magnetization (M_0) and spin system response interacting with external (or internal) magnetic fields. Thus, the general Bloch equation can be used, which is written in the following form:

$$\frac{d\vec{M}}{dt} = \gamma\left(\vec{M} \times \vec{B}\right) - \frac{M_x \cdot \vec{i} + M_x \cdot \vec{j}}{T_2} - \frac{\left(M_z - M_\infty\right) \cdot \vec{k}}{T_1}, \tag{2.1}$$

or, if we project this equation along the three coordinates (Ox, Oy and Oz) we get the set of three Bloch equations:

$$\begin{cases} \dfrac{dM_x}{dt} = \gamma\left(\vec{M} \times \vec{B}\right)_x - \dfrac{M_x}{T_2} \\ \dfrac{dM_y}{dt} = \gamma\left(\vec{M} \times \vec{B}\right)_y - \dfrac{M_y}{T_2} \\ \dfrac{dM_z}{dt} = \gamma\left(\vec{M} \times \vec{B}\right)_z - \dfrac{\left(M_z - M_\infty\right)}{T_1} \end{cases}, \tag{2.2}$$

where the total nuclear magnetization is calculated as $\vec{M}(t)=\sum_{i=1}^{N}\vec{\mu}_i$. N is the number of nuclei in the sample to be measured and $\vec{\mu}_i$ It is the magnetic moment of the nucleus i, where i runs through all the nuclei [30, 31].

2.1.3 CPMG pulse sequence for measuring spin-spin relaxation time, T2

The longitudinal relaxation time, T_1, is most often measured by the technique called *inversion recovery*. A first radio frequency pulse has the 180^0_y effect of rotating the total magnetization (initially in the Oz direction) by 180^o and which after the pulse orients itself along the *-Oz* direction. After the evolution of the spine system over a period of time τ, some of the nuclear spines relaxed.

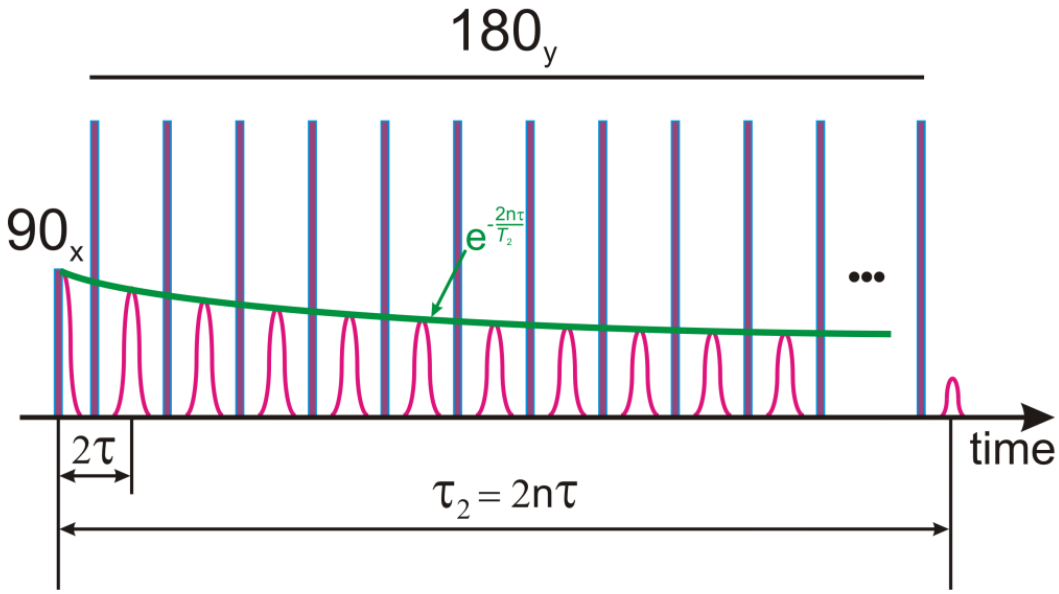

Fig. 2.1. CPMG (Carr-Purcel-Meiboom-Gill) radiofrequency pulse sequence and exponential decrease in the echo train [30, reproduction with permission].

2.1.4 Transforma Laplace

The evaluation of the spin–lattice (longitudinal), T_1 and spin–spin (transverse) T_2 relaxation time distributions can be used to identify and study the different molecular species according to their dynamics. In recent times, new methods of nuclear magnetic resonance have been developed that allow a spine system to evolve under the influence of different relaxation mechanisms, which can lead to the macroscopic properties of these molecular species. These methods are based on the analysis of data measured using the inverse Laplace transform, which in this respect is similar to classical multidimensional MRI spectroscopic methods [30, 32-36].

In general, the Laplace transform represents a practical method of solving certain types of problems that involve different relaxation mechanisms when the initial conditions are given. Thus, the evolution of the magnetization of a spin system is considered as a sum of falls described by several exponential functions having different time constants (T_2). Each of these falls is characterized by a certain weight (or probability) of the total magnetization A(T_2),

$$M(t) = \sum_{i=1}^{N} A(T_{2,i}) e^{\frac{-t}{T_{2,i}}}, \tag{2.3}$$

in general, this equation can be written in the mathematical form of the Laplace transform [30, 32-36]:

$$F(s) = \int_{-\infty}^{+\infty} f(t) e^{-st} dt, \tag{2.4}$$

where for $s = j\omega$ (cu j^2 = -1, imaginary number) the Fourier transform is obtained. So, it can be said that the Fourier transform is the Laplace transform evaluated only on the imaginary axis. The purpose of using the inverse Laplace transform is to determine, from the measured data, the distribution functions of the relaxation times $A(T_2)$ one-dimensional. The Laplace transform can also be successfully applied to identify multidimensional correlation functions (such as parametric maps T_2 - T_2 și T_1 - T_2).

2.2 FT-IR Spectroscopy

Infrared spectroscopy is one of the modern methods (along with NMR spectroscopy and mass spectrometry) that allows, through spectral analysis, to identify the types of molecules that are present in a sample but also their concentration. In the world, there are several types of infrared spectrometers, but the most widely used is the FT-IR type. The term FT-IR comes from the words Fourier Transform Infrared. In this case, the appropriate term used to describe light is as a form of electromagnetic radiation. Thus, light, as an electromagnetic wave, is considered to be composed of electric and magnetic oscillations represented by the electric field vector and the magnetic field vector. The distance traveled by a wave during a cycle (a period) is called the wavelength, for which the Greek letter lambda is used (λ). Another important property of an electromagnetic wave (light or especially in the infrared range) is the wavenumber, which is denoted by the letter $\tilde{\nu}$. The wavenumber measures the number of cycles a wave passes through per unit length (1 m). These wave numbers are measured in units of cycles per centimeter, which are frequently abbreviated as cm^{-1} and can be pronounced as reverse centimeters, reciprocal centimeters, or even wave number. Thus, for example, if a spectrum has a peak at 3000 cm^{-1}, it means that the sample has absorbed

infrared light that has undergone 3000 cycles per centimeter. Most spectra measured in the infrared range are plotted on the *x*-axis from left to right from 4000 to 400 cm^{-1}. FT-IR spectrum graphs should always follow this convention [37-42].

The absorbance spectrum of a sample is calculated from the following equation:

$$A = -\log\left(\frac{I}{I_0}\right) = \log\left(\frac{I_0}{I}\right), \quad (2.5)$$

where A is the absorbance, I_0 is the intensity in the background spectrum, and I is the intensity in the sample spectrum (the test to be measured).

Absorbance is related to the concentration of molecules in a sample by means of an equation called *Beer's Law (or Beer-Lambert)*:

$$A = \varepsilon \ell c. \quad (2.6)$$

where, ε is the absorption coefficient, ℓ is the length of the path and c is the concentration of the solution.

Fig. 2.2. a) Sample preparation for FT-IR spectroscopy measurements and (b) Jasco 6200 FT-IR spectrometer used in experimental studies.

2.3 UV-VIS Spectroscopy

Among other techniques, such as determination of melting point, refractive index, and density, ultraviolet radiation and visible light optical spectroscopy (UV-VIS) is widely applied in almost all workplaces in research, production, and quality control for the classification and study of substances. UV-VIS spectroscopy is based on the absorption of light by a sample of interest. Depending on the amount (flux) of light and wavelength absorbed by a sample, valuable information such as sample purity or component elements can be obtained. Moreover, the amount of radiation absorbed is related to the mass of the sample, and therefore quantitative analysis is possible by optical spectroscopy. Optical spectroscopy is thus based on the interaction of light with matter [43].

2.4 X-ray diffraction

Crystallography based on the diffraction of incident X-rays on samples, usually powder, is a well-established and widely used method in the field of material characterization to be able to obtain information about the atomic structure of different substances in a variety of states. There have been numerous advances in this field, since the discovery of X-ray diffraction in crystals in 1912 by Max von Laue and in 1913 by W.L. Bragg and W.H. Bragg. The origin of crystallographic methods can be traced back to the first studies of the external appearance of natural minerals. Since then, a large amount of data has been systematized by applying geometry (various projections) and group theory. Thus, crystallography becomes a valuable method for studying how crystals can be built from small units by repeating, indefinitely, identical structural units (elementary cells) in space [44].

Fig. 2.3. a) Sample preparation for XRD; b) and c) SHIMADZU 6000 X-ray diffractometer.

2.5 Scanning Electron Scanning Imaging, SEM

The scanning electron microscope (SEM) has proven to be one of the most versatile tools available for morphology analysis and examination of microstructure and chemical composition characteristics. SEM techniques provide information about topography and surface composition by collecting and processing signals that are generated by *a probe* (beam) of electrons sharpened (focused) in a given volume of interaction. The main advantages can be summarized as follows: 1) firstly, SEM offers an imposing visualization of structures ("imagine to imagination"). This is due to the ability to produce images with high plasticity and almost stereoscopic (with 3D valences) in appearance, and, depending on the imaging conditions, a large depth of focus even for samples with pronounced relief; 2) secondly, there is a huge range of adjustable magnifications from the magnification of the reading magnifier (about 10 times), for example, for the overall mapping of large sampling areas or to identify the regions of interest and the possibility of increasing the range up to a few nanometers, depending on the instrument (standard vs. high

resolution) and the properties of the sample; 3) thirdly, there is the analytical power to obtain information about the composition of the material by selecting signals from specific interactions, such as, for example, characteristic X-ray quanta or backscattered electrons.

Fig. 2.4. a) Sample preparation for SEM analysis b) SEM JEOL JSM 5600LV microscope with scanning.

It is necessary to know some basic principles specific to optical light interference in order to understand the fundamentals of electron microscopy. When the center of two primary peaks is separated by a distance equal to the radius of the disk Airy, then two objects can be distinguished from each other, and the system can be described mathematically by Abbe's equation:

$$d = 0.612\ \lambda / n\ sin\ \alpha, \tag{2.7}$$

where d is the resolution, λ is the wavelength of the characteristic radiation, n is the refractive index of the medium between the point source and the lens, and α is half the angle of the light cone in the specimen plane accepted by the objective (the angle of half the aperture in radians). The term $n \times \sin(\alpha)$ is often called numerical opening (aperture).

Replacing the illumination source and capacitor lens with the electron beam and electromagnetic coils in microscopes leads to the emergence of electronic transmission. The electron transmission microscope (TEM) was first built in 1930 and the electron beam was focused by an electromagnetic condensing lens. Unlike TEM, SEM uses a focused electron beam to scan the surface of the systematic specimen, producing a large number of signals (secondary electrons and characteristic electromagnetic radiation). These electronic signals are eventually converted into a visual signal displayed on the screen as an image [45].

CHAPTER 3 CHARACTERIZATION OF ORGANO-MINERAL FERTILIZERS BASED ON BIOSOLIDS

3.1 One-dimensional nuclear magnetic resonance used for the characterization of organo-mineral fertilizers

Nuclear magnetic resonance is a powerful method for characterizing materials, especially those of organic origin, such as organo-mineral fertilizer based on biosolids. The types of biosolids-based fertilizers produced within the experimental program of the thesis fit very well into this category. One of the capabilities of nuclear magnetic resonance is that several types of pulse sequences can be used to measure different NMR parameters specific to the samples to be studied. One of these sequences of NMR pulses is called *saturation recovery*, and is used to determine the distributions of spin-network relaxation times, T_1 [46, 47].

3.1.1 1D distributions of spin-network relaxation times, T_1

Another valence of nuclear magnetic resonance is that, unlike many other characterization methods, it can provide us with distributions of the measured parameters and not just a value that characterizes the measured samples globally [48, 49]. Figure 3.1 shows the distributions of the T_1 relaxation times for the three fertilizers V1, V2 and V3 produced, and whose component elements are presented in Table 1.1. Quite large similarities of the distribution curves of T_1 can be observed for fertilizers V2 and V3, while the sample V1 shows a different distribution of relaxation times T_1.

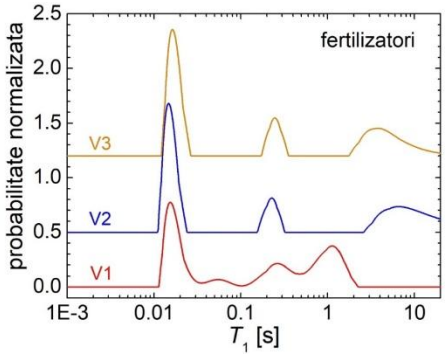

Fig. 3.1. Distributions of T_1 longitudinal relaxation times for the three types of biosolids [21].

3.1.2 1D distributions of spin-spin relaxation times, T_2

Figure 3.2. shows the distributions of the spin-spin relaxation time measured for the fertilizers obtained with the V1, V2 and V3 preparation recipes. There are some specific variations and a difference from the distributions obtained for T_1 relaxation times. Broadly speaking, these peaks can be associated with components with different dynamics and containing hydrogen. Thus,

at low values of T_2 one could find components of these fertilizers that contain hydrogen and are rigid (have reduced mobility).

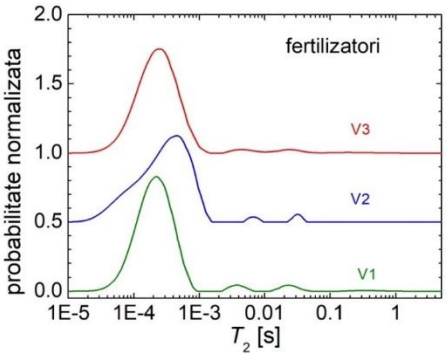

Fig. 3.2. Transverse relaxation time distributions T_2 for the three types of biosolids [21].

3.1.3 1D distributions of dipole residual coupling

An advanced method in nuclear magnetic resonance is that of using the signal coming from coherences of several quanta. The most commonly used are two-quantum coherences. These require that at least two nuclear spins of hydrogen (because this is the spin measured by nuclear magnetic resonance, using a Bruker Minispec spectrometer) are coupled. Thus, two-quantum measurements act as a filter for isolated spins, and only coupled spins, which are most likely found in rigid components, induce an NMR signal in the receiving coil.

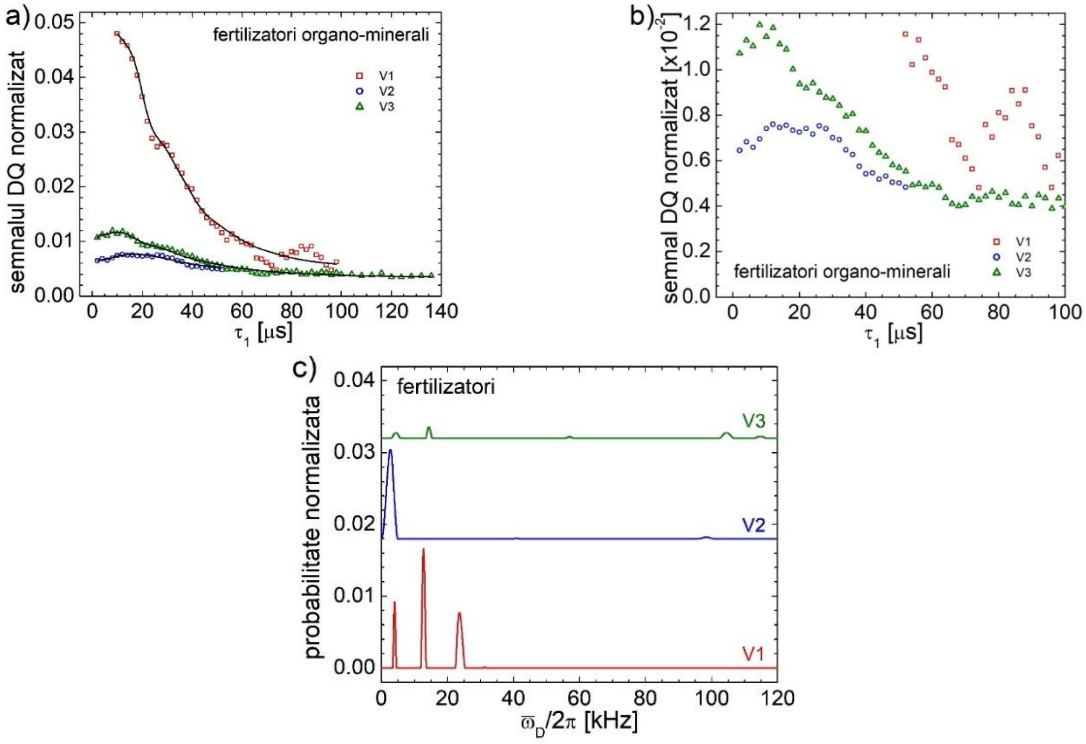

Fig. 3.3. Two-quantum growth and decrease curves measured for fertilizers V1, V2 and V3 presented a) at normal scale and b) increased, and c) Distributions of dipole residual couplings, measured for the three types of biosolids in the two-quantum curves presented in (a) $\bar{\omega}_D$[21].

3.1.4 NMR spectra of ^{1}H and ^{13}C under MAS

Spectra ^{1}H and ^{13}C NMR measured for organo-mineral fertilizers V1, V2 and V3 recorded under MAS conditions are shown in Figures 3.4 and 3.5. As a general characteristic, similarities between the measured spectra can be observed, indicating a similar molecular structure. They consist of a small, wide peak, centered at ~15.27 ppm. The amplitude of this peak measured for fertilizer V2 is much lower, compared to the amplitude of the peaks measured for V1 and V3. Then a relatively narrow peak can be observed, centered at ~6.89 ppm, with a long tail extended to about 15 ppm. A small shoulder occurs for all three spectra at about 1.93 ppm.

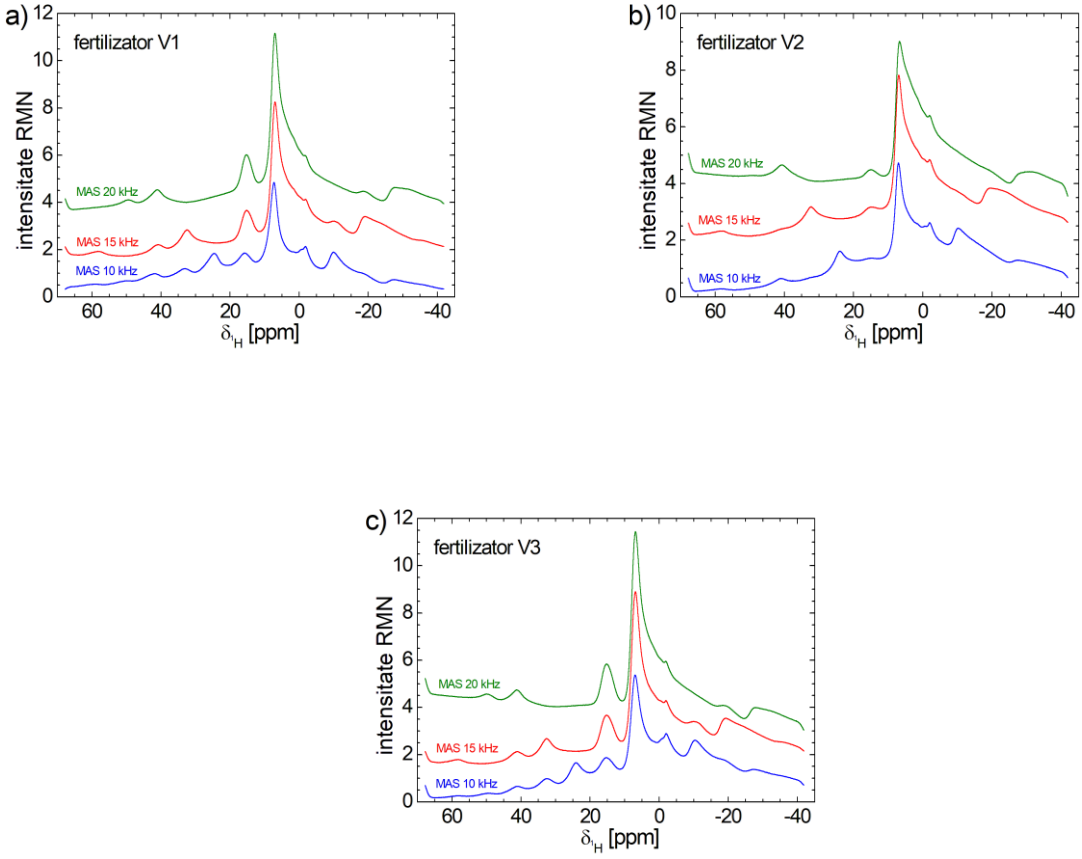

Fig. 3.4. NMR spectra of ^{1}H measured for fertilizers a) V1, b) V2 and c)V3 below MAS at frequencies 10, 15 and 20 kHz [21].

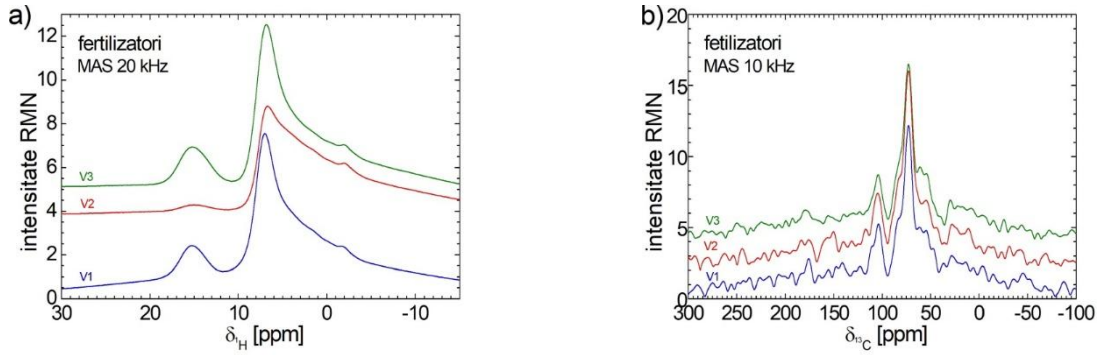

Fig. 3.5. NMR spectra of (a) ^{1}H measured below MAS at 20 kHz and (b) ^{13}C measured below MAS at 10 kHz for organo-mineral fertilizers V1, V2 and V3 [21].

3.2 Characterization of organo-mineral fertilizers by FT-IR spectroscopy

Fourier transform infrared spectroscopy (FT-IR) is a modern method capable of identifying the structure of simple samples or, if the measured sample is more complex, providing detailed information about the type of chemical bonds. Figure 3.6 shows the FT-IR spectra measured for the three fertilizers produced collaboratively in this thesis. A great similarity between these spectra can be observed, but there are also major specific differences between them. Thus, for the analysis of FT-IR spectra, the focus is on two areas of interest. The first zone is in the range of about 2600 to 3800 cm^{-1}, where there is a wide peak associated with water, and shows some small maximums at about 2737-2741 cm^{-1} (associated with the vibrations of the extension of the N-H bond in NH_3^+), 2873-320 cm^{-1} (associated with the symmetrical vibrations ν_s of CH_3, and with those of the extension of the bonds in C-H, N-H), 2933-2945 cm^{-1} (associated with C-H stretch bands, and with the asymmetric vibrations ν ace in CH_2), 3124-3127 cm^{-1} and 3241-3244 (associated with the symmetrical O-H stretch belonging to water that is intrinsically found in the measured samples or can be hygroscopically absorbed as moisture from the air) [50, 51].

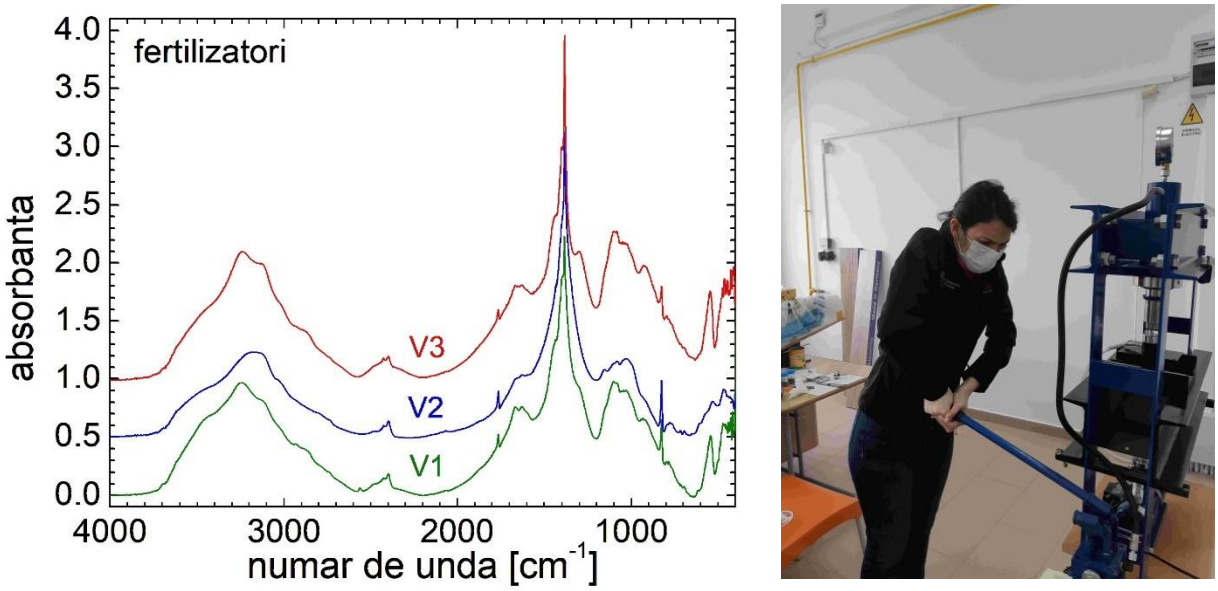

Fig. 3.6. a) FT-IR spectra of V1, V2 and V3 samples and (b) Sample preparation for FT-IR measurements [21].

3.3 Characterization of organo-mineral fertilizers by SEM, EDX and DRX

If FT-IR analysis can identify structures at the molecular level (through chemical bonds), scanning electron microscopy (SEM) and models obtained from X-ray diffraction (XRD) can provide information about structural organization at the nano to micrometer level [56]. Thus, SEM-EDX (SEM-localized energy dispersive spectroscopy) images are shown in Figure 3.7 for all three fertilizer types V1 (top), V2 (middle) and V3 (bottom). In the left column is shown a colored map (*folder*) that overlaps with SEM images of a submillimeter-sized area of each type of fertilizer. The colored pixels indicate the presence of particular elements and can be associated as follows: i) red with iron (Fe); ii) light blue with potassium (K-kalium); iii) orange with sulfur (S); iv) light red with phosphorus (P); v) pink with silicon (Si); vi) dark blue with aluminum (Al); vii) yellow with oxygen (O); viii) green with nitrogen (N); ix) carbon blue (C). The EDX spectra recorded for the SEM images on the left are shown in the right column.

V1

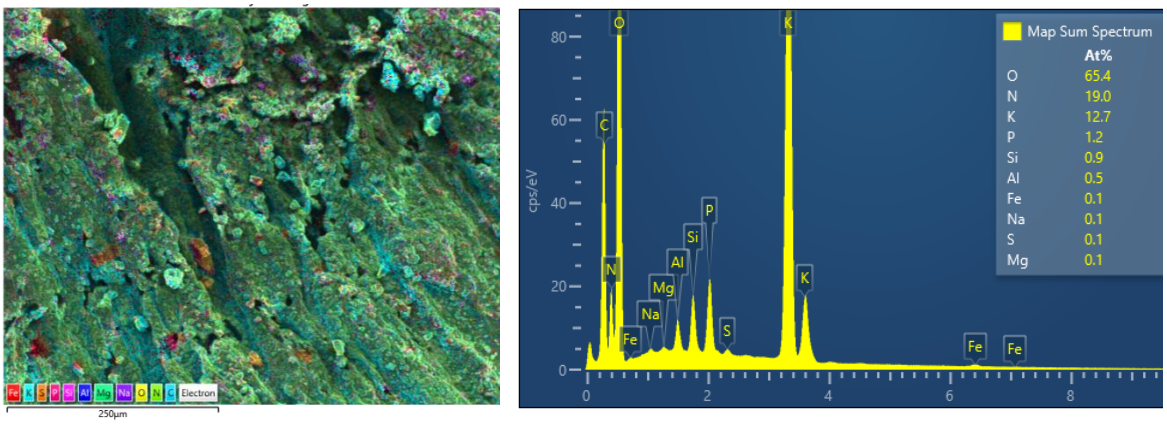

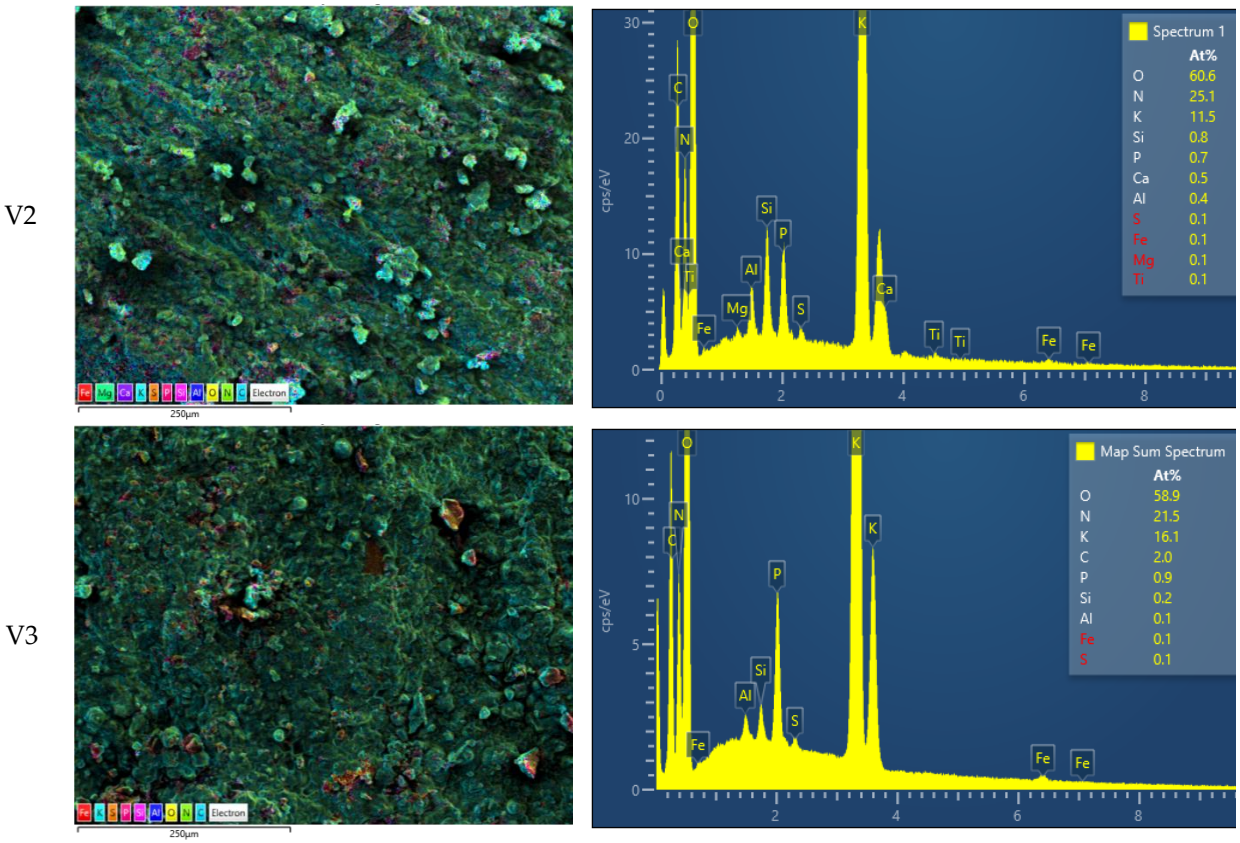

Fig. 3.7. SEM – EDX of the most abundant elements in fertilizers V1, V2 and V3 (left) and EDX spectra measured from EDX maps (right) [21].

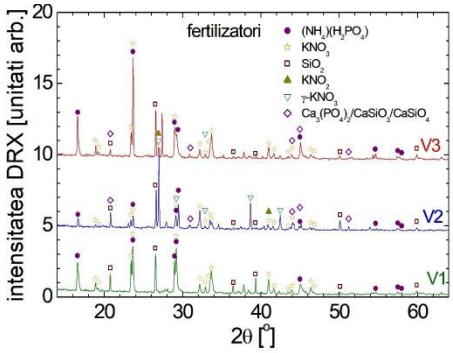

Fig. 3.8. X-ray diffractogram measured for fertilizer samples V1, V2 and V3 [21].

CHAPTER 4 CONSTRUCTION OF THE *ELECTROSPINNING DEVICE*

4.1 Component elements

The electrospinning device was designed and manufactured on a small scale within the experimental program of this doctoral thesis, in order to be able to produce samples from different types of solutions but also to be able to optimize the process parameters, thus offering the possibility to obtain different types of nanofibers. The components of the electrospinning machine include a number of essential components, each of which plays an important role in the production and collection of fibers. The design of some components of the electrospinning machine was carried out with the help of the SolidWorks design program and then printed on a 3D printer located within the Laboratory of Nuclear Magnetic Resonance and Sensor Physics of the Technical University of Cluj-Napoca. The protective camera was the most complex element and was designed for the safety of the user and for maintaining an environment as stable as possible in terms of temperature and humidity. In Figure 4.1 the final version of the electrospinning machine made in the laboratory can be seen. This device has two levels, the lower level comprises the electrical part and the injection pump, and the upper level comprises the metal needle with the help of which the solution is released and collected by the rotating reel as well as the support for the metal needle, the rotating reel and the motor.

Fig. 4.1. Electrospinning machine .

4.2 Electrospinning machine construction

The construction of the *electrospinning* machine took place in several stages. In the first phase, the protection chamber consisting of the two levels was installed. On the first level, all the electrical elements (the high voltage source and the engine power supply) were placed, as well as the injection pump (the medical injector). All these elements are protected by the fiber production area. In the fiber production area, it was necessary for the upper level to be airtight due to the toxic vapors that are formed.

Fig. 4.2. Stages of the electrospinning device construction process .

CHAPTER 5 Production of nanofibers by *electrospinning*

5.1 Materials and methods for the production of nanofibers by *electrospinning*

5.1.1 Materials

The raw materials used for the production of nanofibers by electrospinning are shown in Figure 5.1 and have been purchased from different manufacturers. Thus, peptide collagen, from land animals, was produced by Arkure Health Care (India, Rohtak).

Fig. 5.1. Raw materials used for the production of nanofibers by electrospinning.

5.2 Production of chitosan-based nanofibers

The production of chitosan nanofibers through the electrospinning process involves transforming the chitosan solution into a fibrous material at the nano-scale. For the production of these chitosan-based fibers, since chitosan does not dissolve in pure water, it was necessary to introduce solvents such as acetic acid or formic acid for the formation of the solution. The acid was diluted in distilled water with different percentages. The nanofibers produced from the chitosan-based solution were collected on the aluminum foil on the spinning drum (see Fig. 5.5) and then carefully detached. In Figure 5.2 b) some of the nanofibers obtained from the electrospinning process can be seen.

In order to simplify the detachment of the nanofiber film deposited on the aluminum foil, a gauze wound only on a portion of the rotating drum was used. Visually, the film produced has a slightly yellowish and translucent color, and to the touch the chitosan film formed has a smooth, flexible texture and an extremely fine surface. This film has a structure that can mimic the texture and mechanical properties of biological tissues. Because chitosan has better mechanical strength than other natural polymers, chitosan solution has been used in several combinations to improve the properties of other natural polymers such as gelatin or collagen.

Fig. 5.2. Obtaining chitosan-based nanofibers.

5.3 Production of PVA-based nanofibers

The introduction of a synthetic material into the *electrospinning* process can help form nanofibers with a much better mechanical structure [53]. In the first stage, we wanted to introduce a synthetic material such as PVA (polyvinyl alcohol). The preparation of the solution for electrospinning is similar to the method used to form solutions based on natural polymers. The solvent used in this process was also acetic acid in a concentration of 90%, but the dissolution of the polymer could not be done at the temperature of 40^{o} C, so the temperature was increased to 60^{o} C. The temperature of 60^{o} C was used in all variants produced based on PVA, and in total 3 variants based on PVA with different concentrations (100 %, 50 % and 10 %).

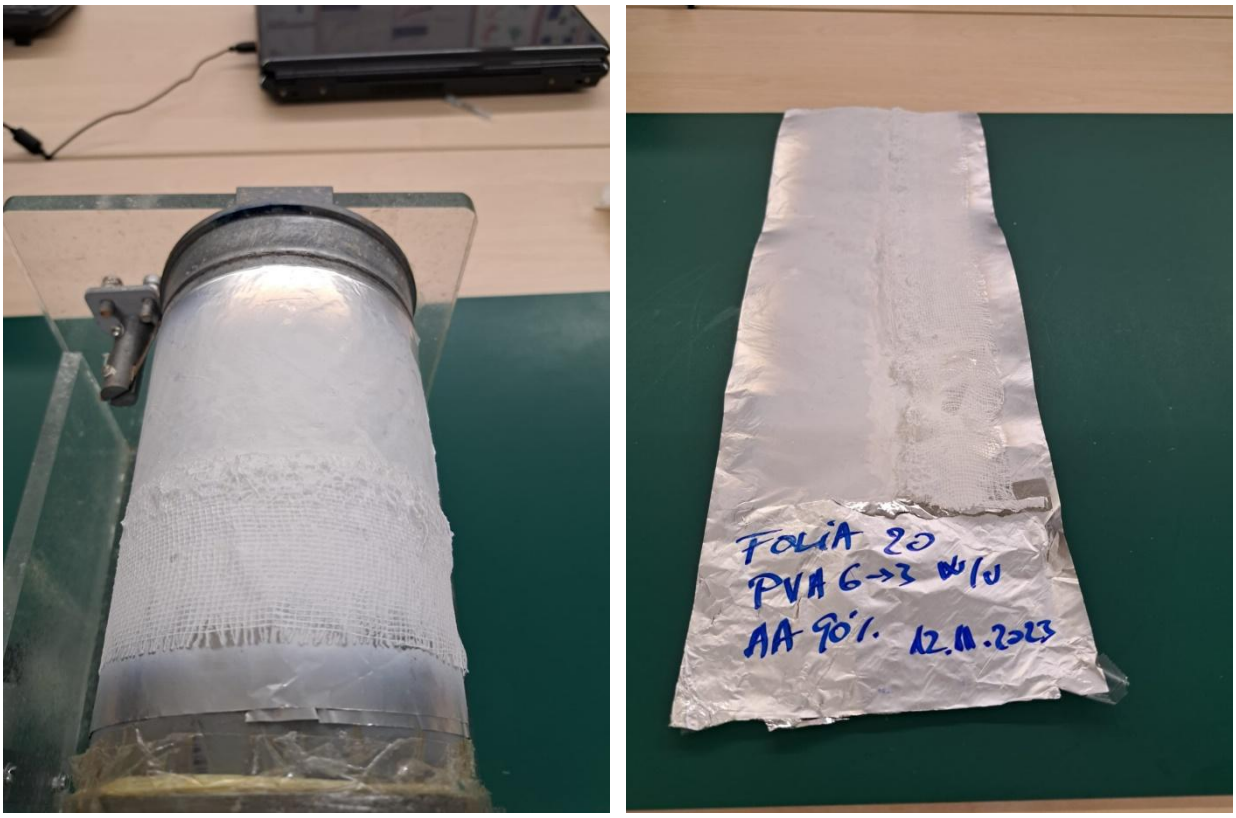

Fig. 5.3. Obtaining PVA-based nanofibers.

The PVA solution was mixed with chitosan solution (50 % and 90 %). The PVA solution does not have a very high viscosity but mixed with the chitosan solution, the viscosity has increased relatively much. The parameters used for the production of PVA and chitosan-based fibers were different. The texture of the resulting PVA-based fibers has a network of very thin fibers, fine to the touch. These fibers are highly resistant to tearing and have greater elasticity than fibers made from natural polymers [53]. The resulting foil is white in color as can be seen in Figure 5.3, and the detachment of the foil from the drum did not involve any difficulties.

Table 5.1. Nomenclature of solutions used for the production of bio-nanofiber films by electrospinning.

Nomenclature of solutions used for electrospinning and film production	Solution 1		Solution 2		Solution 1 /Solution 2
	Polymer 1 [%]	Solvent 1 [%]	Polymer 2 [%]	Solvent 2 [%]	
Ch6AA60	Chitosan 6% w/v	Acid Acetic 60 %	-	-	100/0
Ch6AA90	Chitosan 6% w/v	Acid Acetic 90 %	-	-	100/0
Col6AA05	Colagen 6% w/v	Acid Acetic 05 %	-	-	100/0
Ch6AA90(90):Col6AA05(10)	Chitosan 6% w/v	Acid Acetic 90 %	Collagen 6% w/v	Acid Acetic 05 %	90/10
Ch6AA90(50):Col6AA05(50)	Chitosan 6% w/v	Acid Acetic 90 %	Collagen 6% w/v	Acid Acetic 05 %	Stra1/stra2
FG6H_2O100	Fish gelatin 6% w/v	H_2O 100 %	-	-	100/0
Ch6AA90(90):FG6H_2O(10)	Chitosan 6% w/v	Acid Acetic 90 %	Fish gelatin 6% w/v	H_2O 100 %	90/10
Ch6AA90(50):FG6H_2O(50)	Chitosan 6% w/v	Acid Acetic 90 %	Fish gelatin 6% w/v	H_2O 100 %	50/50
PVA6AA90	PVA 6% w/v	Acid Acetic 90 %	-	-	100/0
Ch6AA90(90):PVA6AA90(10)	Chitosan 6% w/v	Acid Acetic 90 %	PVA 6% w/v	Acid Acetic 90 %	90/10
Ch6AA90(50):PVA6AA90(50)	Chitosan 6% w/v	Acid Acetic 90 %	PVA 6% w/v	Acid Acetic 90 %	50/50
PEG6AA90	PEG 6% w/v	Acid Acetic 90 %	-	-	100/0
Ch6AA90(90):PEG6AA90(10)	Chitosan 6% w/v	Acid Acetic 90 %	PEG 6% w/v	Acid Acetic 90 %	90/10
Ch6AA90(50):PEG6AA90(50)	Chitosan 6% w/v	Acid Acetic 90 %	PEG 6% w/v	Acid Acetic 90 %	50/50

CHAPTER 6 CHARACTERIZATION OF THE PROPERTIES OF RAW MATERIALS USED FOR THE PRODUCTION OF NANOFIBERS BY ELECTROSPINNING

6.1 ^{1}H NMR relaxometry

Chitosan is characterized by a semi-rigid component characterized by a peak in the T_2 distribution located at $T_2 \approx 2.91$ ms and a semi-mobile component with a spin-spin relaxation time at $T_2 \approx 23.18$ ms. Collagen peptide is characterized by three less rigid components, two semi-rigid components with relaxation times located at $T_2 \approx 2.31$ and, respectively, at $T_2 \approx 10.9$ ms and one semi-mobile with $T_2 \approx 57.0$ ms. Similarly, marine fish collagen is also characterized by three less rigid components, two semi-rigid components with $T_2 \approx 1.74$ ms and $T_2 \approx 14.8$ ms respectively, and one semi-mobile component with $T_2 \approx 58.6$ ms. Except for one component (with T_2 located at about 2 ms), the rest of the components of marine fish collagen are more mobile compared to the corresponding components of the collagen peptide.

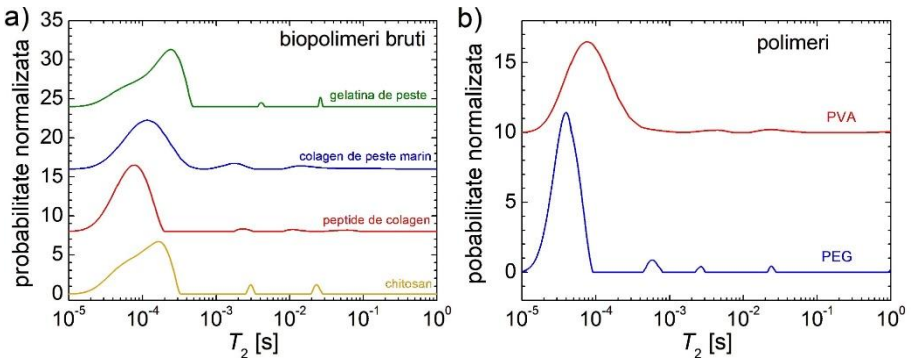

Fig. 6.1. Distributions of T_2 measured by NMR of ^{1}H for crude biopolymers a) chitosan - orange, marine fish collagen - blue, collagen peptide - red and fish gelatin - green and b) PEG and PVA polymers used for electrospinning [53].

6.2 FT-IR spectroscopy

Figure 6.2a in orange (bottom) shows the FT-IR spectrum measured in the chitosan experimental program. This (FT-IR spectrum) exhibits a strong and wide band in the region of 3297 cm^{-1} that can be associated with the stretching of the N-H and O-H bonds, but also with the intra-molecular hydrogen bonds and is localized in amide A. This widening is evidenced by overlapping with another wide peak located at about 3200 cm^{-1}. A strong peak was observed at 2924 cm^{-1} which pairs with the peak located at 2855 cm^{-1} belonging to amide B and which can be attributed to the symmetrical and asymmetrical stretches of C-H, respectively. This doublet is found in many organic samples (see also collagen-based spectra), especially those of polysaccharides, such as carrageenan [54], xylan [55], and glucans [56].

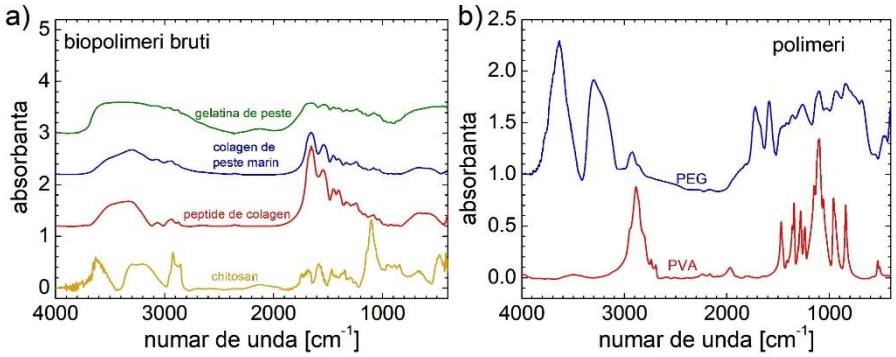

Fig. 6.2. FT-IR spectra of crude biopolymers a) chitosan - orange, marine fish collagen - blue, collagen peptide - red and fish gelatin - green) and b) PEG and PVA polymers used for electrospinning [53].

6.3 X-ray diffraction

For the structural characterization of the raw bio-materials used for the production of electrospun nanofibers, XRD diffractograms were recorded [57] and are shown comparatively in Figure 6.3. Similarities can be observed between the X-ray diffractograms recorded for marine fish collagen, collagen peptide, and fish gelatin that exhibit an amorphous structure with wide peaks centered at $2\theta \approx 20.46^{o}$ for marine fish collagen, the $2\theta \approx 20.64^{o}$ for collagen peptide and to $2\theta \approx 20.11^{o}$ for fish gelatin. For marine fish collagen, a peak (the smallest) can also be observed, like a left shoulder. By applying a deconvolution procedure of the X-ray diffractogram measured for the collagen sample, it is observed that it can be decomposed (ad-hoc) into three broad peaks centered at $2\theta = 11.82^{o}$, 20.36^{o}, 23.60^{o}, and widths of 4.45^{o}, 7.74^{o} și 27.23^{o}, and the relative integral areas of 4.85 %, 31.25 % and respectively, 63.91 %.

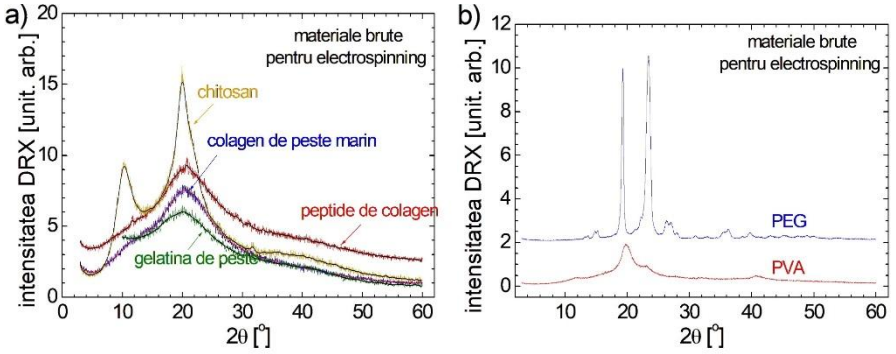

Fig. 6.3. X-ray diffractograms of raw materials a) chitosan (orange), marine fish collagen (blue), collagen peptide (red) and fish gelatin (green) [53] and b) PEG and PVA polymers used for electrospinning.

CHAPTER 7 CHARACTERIZATION OF SOLUTIONS FOR THE PRODUCTION OF NANOFIBERS BY ELECTROSPINNING

7.1 The effect of collagen distortion in acetic acid solutions with different concentrations

In order to evaluate the denaturation effect on marine fish collagen, within the experimental program of this doctoral thesis, different solvent solutions from glacial acetic acid (AA) were prepared. The concentration of acetic acid was chosen in the range of 5 % to 90 %. Marine fish collagen was dissolved in each of these reagents and for the resulting solutions the MRI spectra of ^{1}H and FT-IR were measured [58], spectra that are shown in Figure 7.1. Thus, in Figure 7 1a, the NMR spectra of ^{1}H measured for solutions of 6 % w/v collagen dissolved in acetic acid with concentrations of 5 %, 10 %, 20 and 40 %, and the NMR intensities are presented at full scale (vertical). The MRI spectra of ^{1}H were measured using an MRI tomograph in high fields (7 T), using a localized spectroscopy procedure that allows water suppression (the peak from the water resonance at $\delta \approx$ H 4.65 ppm is suppressed experimentally, with high efficiency).

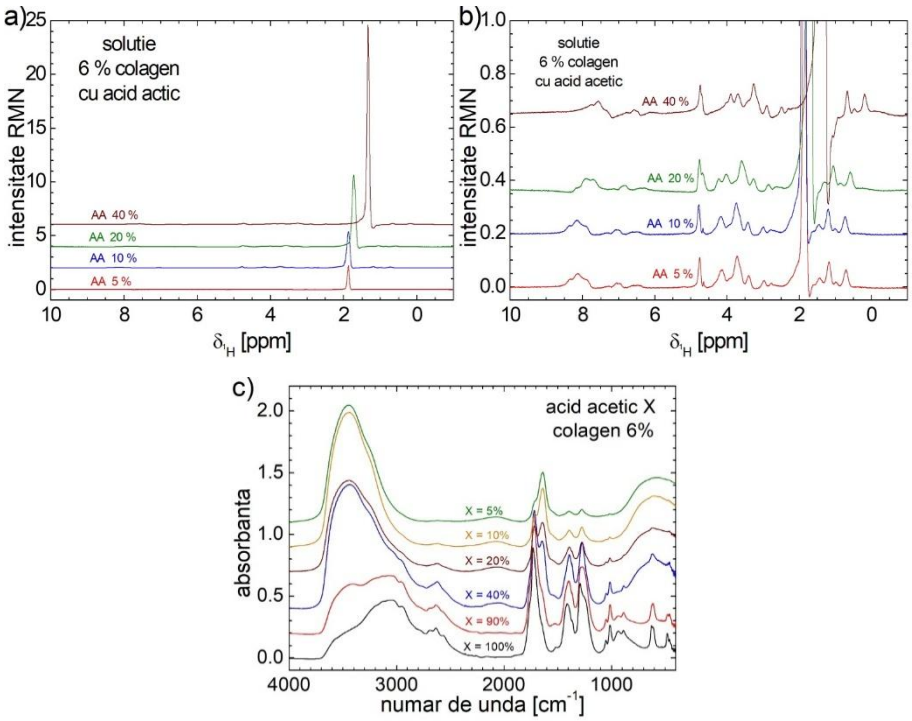

Fig. 7.1. NMR spectra of ^{1}H measured in high fields using localized spectroscopy and water filtration represented at a) actual NMR intensity and b) increased NMR intensity and c) FT-IR spectra used to determine collagen distortion in acetic acid solutions with different concentrations from 5 % to 100 % [53].

7.2 NMR spectroscopy of ^{1}H in high fields

In the previous subchapter it was shown that too high a concentration of acetic acid can lead to collagen denaturation. This effect has also been discussed extensively in reference [53]. It has been found that if collagen dissolved in acetic acid solution is used, then 10-20% acetic acid can begin to cause collagen denaturation, which prevents the formation of fibers [53]. However, if the solution is combined with another (e.g. chitosan-based), then nano-sized fibers can be obtained. The effect of acetic acid concentration on collagen can be easily observed by comparing the NMR spectra of localized ^{1}H, measured in high magnetic field. These are shown at the bottom of Figure 7.2a for samples labeled with Ch6AA90 and Ch6AA60. In the range from $\delta_{^1H} \approx 4.0$ ppm at $\delta_{^1H} \approx 6.0$ ppm peaks specific to suppressed water can be observed.

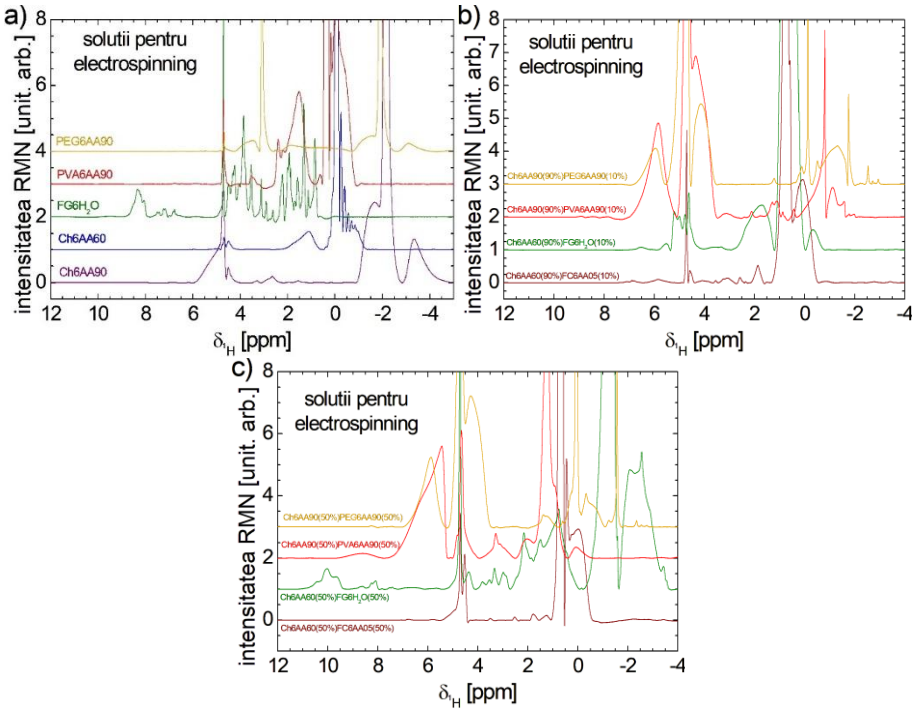

Fig. 7.2. NMR spectra of ^{1}H measured in high fields for a) pure acetic acid solution (90% or 60% and distilled water) and 6% w/v chitosan, fish gelatin PVA and PEG; b) 90% solution 1 of 6% w/v chitosan (AA 90% or 60%) and 10% of solution 2 of 6% w/v marine fish collagen (AA 5%), fish gelatin (100% distilled water), PVA (AA 90%) and PEG (AA 90%); c) solution 1 (50%) of 6% w/v chitosan (AA 90% or 60%) and 50% of solution 2 of marine fish collagen 6% w/v (AA 5%), fish gelatin (100% distilled water), PVA (AA 90%) and PEG (AA 90%) [53].

7.3 Distributions of relaxation times T_2

The dynamics of bio-polymers change completely once they are dissolved in acetic acid or even in plain distilled water. This is demonstrated by the transverse relaxation time distributions T_2, measured for solutions prepared for electrospinning, as shown in Figure 7.3. The main peak (associated with the largest hydrogen tank) is located at higher T_2 values, on the order of hundreds

of milliseconds. The distributions of T_2 are recorded with two echo times (TE). Thus, a small echo time, TE (see T_2 distributions shown on the left of Figure 7.3 – a and c) will ensure the encoding of components characterized by reduced mobility, but at the same time it cannot well resolve peaks that occur at higher T_2 values (usually greater than 100 ms). These are solved when the experimental parameter, the echo time, is set to a higher value (TE = 0.5 ms – see T_2 distributions shown to the right of Figure 7.3 – b and d and the CPMG (Carr-Purcell-Meiboom-Gill) echo train falls close to the baseline. But at the same time, such a high echo time acts as a filter, and the less mobile component is mobile from the NMR signal and no longer appears in the distributions of T_2.

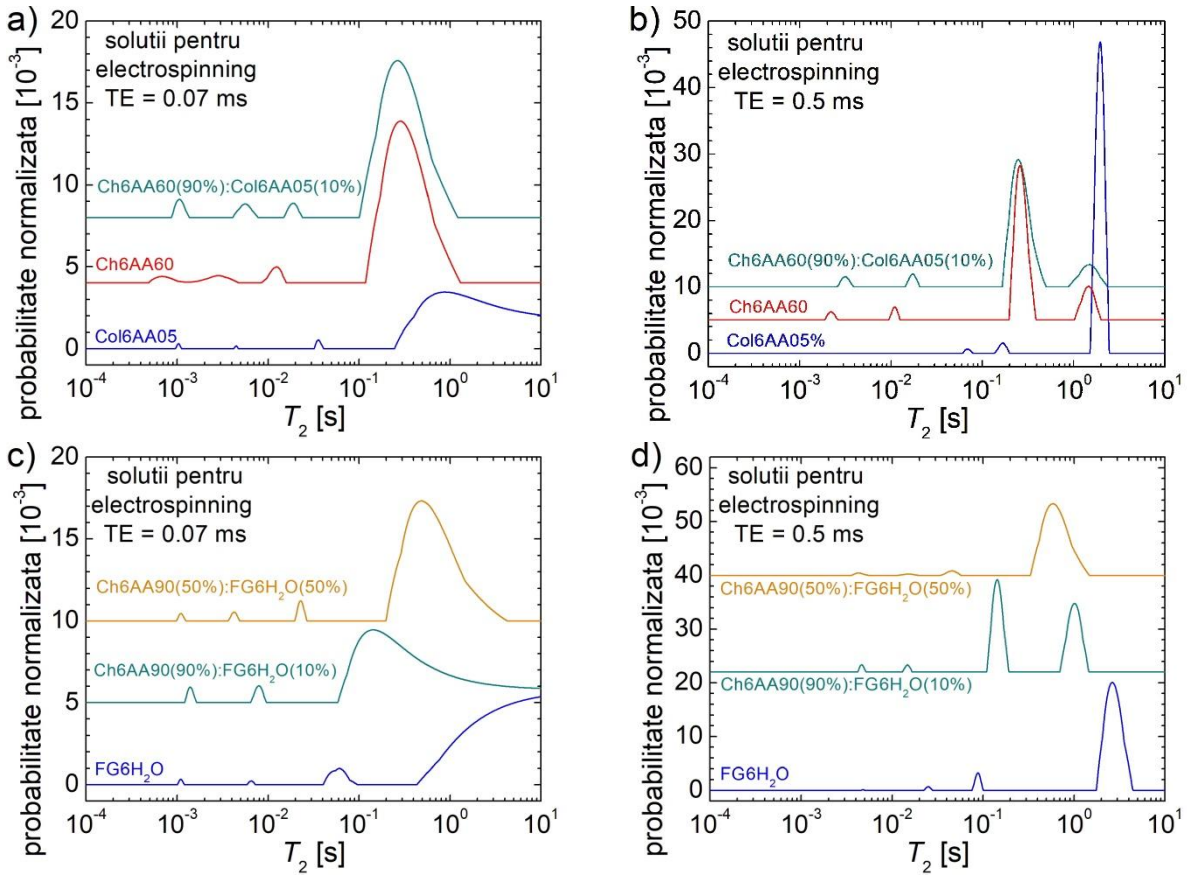

Fig. 7.3. NMR relaxation time distractbtions of ^1H T_2 measured for solutions used for chitosan and collagen-based electrospinning from marine fish (top) and fish gelatin (bottom) using an echo appearance time TE = 70 s (left) and TE = 500 μs (right).

7.4 FT-IR spectroscopy

The interaction between 6 % w/v chitosan to 60 % acetic acid (Ch6AA60) and 6 % w/v collagen to 5 % acetic acid (Col6AA05) is not as complex as expected; this is a result of the FT-IR spectra shown in Fig. 7.4a. These spectra (orange and red in Fig. 7.4a) are mainly superpositions of the spectra recorded for the separate solutions (and discussed largely earlier), but they also exhibit some new features. In this regard, it can be noted that the peak corresponding to water is

part of a large band with the main characteristics that come from the presence of acetic acid (see the black spectrum in Fig. 7.1c). Comparing the FT-IR spectrum recorded for the two-component solution of Ch6AA60(90%)Col6AA05(10%) (orange spectrum in Fig. 7.4a) with that recorded for the two-component solution of Ch6AA60(50%)Col6AA05(50%) (red spectrum in Fig. 7.4a) it can be seen that the difference in acetic acid content, in favor of the former, leads to an increased broadband absorption in the range of 3000-4000 cm^{-1}. The presence of chitosan is barely noticeable by the appearance of extremely small doublets located at about 2844 cm^{-1} and 2788 cm^{-1}, and especially by small noisy series of small peaks extended in the range of 3800-4000 cm-1, and in the range of 1475-1580 cm^{-1}. The greatest effect of chitosan is expected to occur at about 1100 cm^{-1}, but there is an overlap with the group of absorption lines belonging to acetic acid.

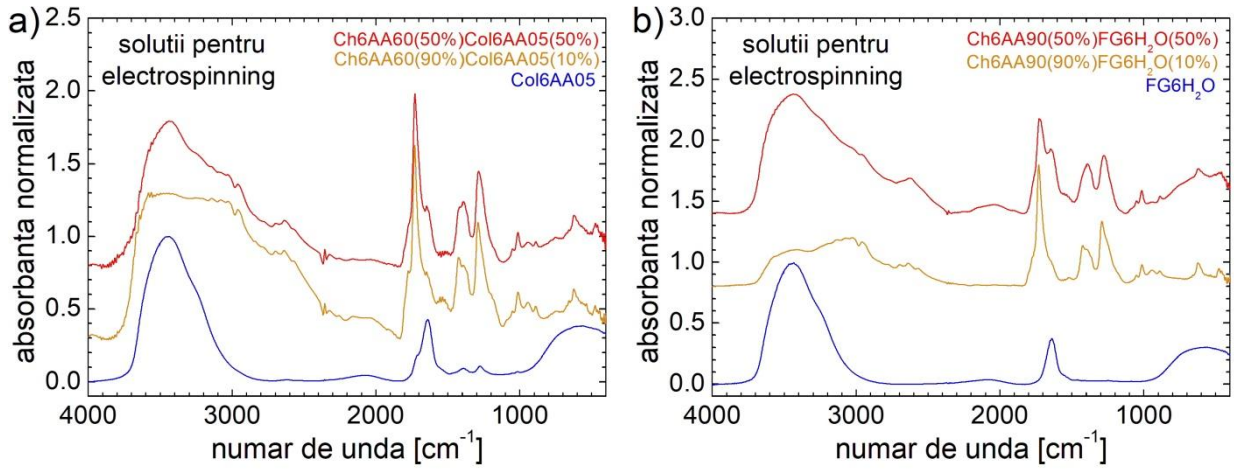

Fig. 7.4. FT-IR spectra of electrospinning solutions prepared on the basis of a) collagen and chitosan and b) fish gelatin and chitosan.

CHAPTER 8 CHARACTERIZATION OF THE PROPERTIES OF NANOFIBERS PRODUCED BY ELECTROSPINNING

8.1 Modern NMR methods for the characterization of nanofibers

8.1.1 ^{1}H NMR Relaxometry

The T_2 distributions measured for all electrospun bio-nanofiber films are shown comparatively in Fig. 8.1. Comparing these distributions of T_2 with those reported in the previous chapters, it can be seen that they (Fig. 8.1) are more similar to those measured for raw materials (Fig. 6.1). The largest amount of hydrogen is found in components with extremely low mobility. This is a general characteristic valid for all electrospun bio-nanofiber films and results from the presence of main peaks (with the largest integral area) located at T_2 values less than 1 ms. With one exception, all T_2 distributions are characterized by a main peak and a series of three other small peaks at T_2 values which indicates greater mobility. The exception is the bio-nanofiber film produced by electrospinning from FG_6H_2O, a solution prepared by dissolving fish gelatin in distilled water. In this case, a series of two main peaks located at lower T_2 values and two other peaks located at higher T_2 values can be observed.

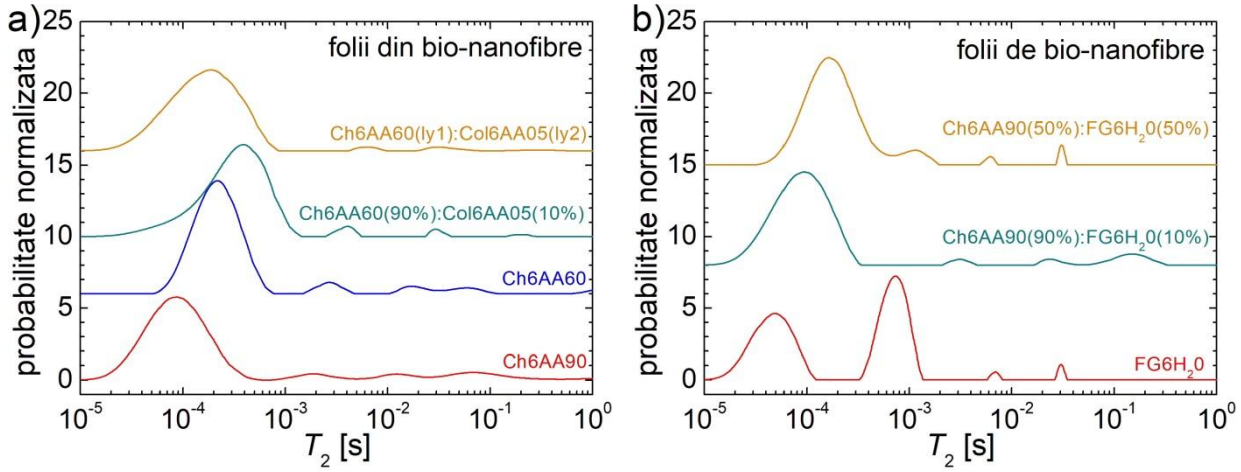

Fig. 8.1 NMR relaxation time distributions of ^{1}H, T_2 measured for bio-nanofiber films obtained by electrospinning from solutions prepared based on a) collagen and chitosan and b) fish gelatin and chitosan [59].

8.1.2 T_2-T_2 EXSY exchange maps

Although promising, the one-dimensional (1D) distributions of T_2 measured by NMR cannot provide a complete picture of the dynamics of the polymer network of the bio-nanofiber films produced by electrospinning which, at the molecular level, form the basic structure. If it is assumed that the solvent (acetic acid, water) is not completely evaporated during the electrospinning process, if the eventual crosslinking (chemical and/or physical) is not permanent,

then a two-dimensional ^{1}H NMR measurement of the T_2-T_2 EXSY type (Laplace-Laplace exchange spectroscopy) can provide valuable information [60, 61].

In Fig. 8.2 are shown four T_2-T_2 EXSY maps recorded for two electrospun films of bio-nanofibers based on chitosan and marine fish collagen and two based on fish gelatin (one also with chitosan) with an exchange time, τ_{mix} = 20 ms. In Fig. 8.2 a) is shown the ^{1}H NMR map of type T_2-T_2 EXSY recorded for Ch6AA90(90%)Col6AA05(10%) exhibiting: i) four clear extra-diagonal peaks describing the molecular exchange process from a ^{1}H reservoir characterized by high T_2 values to a ^{1}H reservoir characterized by lower T_2 values; and ii) an extended peak describing a molecular exchange process from a ^{1}H reservoir characterized by low T_2 values to a hydrogen reservoir with higher T_2 values.

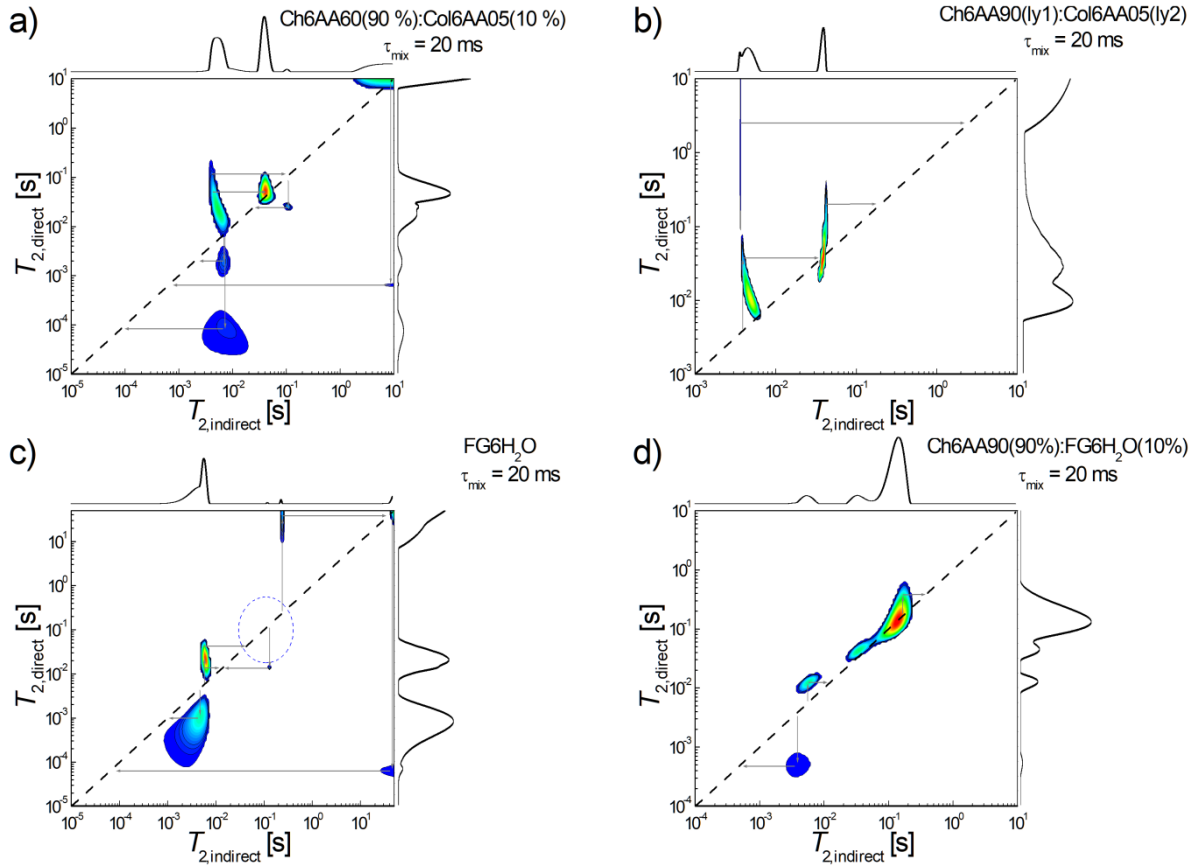

Fig. 8.2. Two-dimensional ^{1}H NMR spectra of the T_2-T_2 EXSY type (exchange Laplace spectroscopy) measured for electrospun bio-nanofiber films from solutions of a) chitosan 6% w/v in acetic acid 60 % (sol-1 90 %) and collagen 6% w/v in acetic acid 5 % (sol-2 10 %); b) chitosan 6 w/v in acetic acid 60 % (layer 1) and marine fish collagen 6% w/v in acetic acid 5 % (layer 2); c) fish gelatin 6% w/v in distilled water and d) chitosan 6% w/v in acetic acid 90 % (sol-1 90 %) and fish gelatin 6% w/v in distilled water (sol-2 10 %) [53].

8.2 Structural characterization of nanofibers by FT-IR spectroscopy

The molecular structure of bio-nanofibers produced by electrospinning is different from the constituents in solutions, as can be seen from the FT-IR spectra shown in Fig. 8.3. Thus, Fig. 8.3a shows the FT-IR spectra recorded for chitosan/collagen-based bio-nanofiber films. The effect of the different concentration of acetic acid in the precursors of bio-nanofiber films produced in the experimental program can be directly observed by comparing the spectra recorded for Ch6AA90 (red - bottom) and Ch6AA60 (blue - bottom). Thus, in the range of specific characteristics (350-1900 cm^{-1}) only small differences between these two samples can be observed. Likewise, in the range 2000-4000 cm^{-1}, where wide peaks occur, some relatively minor differences are observed. Thus, the amplitude variation of the doublet located at approximately 2896 and 2950 cm^{-1} can be observed. It can also be noted that for the sample that initially contained the highest amount of acetic acid, the FT-IR spectrum of the electrospun bio-nanofibers shows a peak of about 1724 cm^{-1} that can be attributed to acetic acid (see the red spectrum in Fig. 8.3a and the black FT-IR spectrum at the bottom of Fig. 7.1c). A similar FT-IR spectrum was also recorded for electrospun bio-nanofibre film made from a solution containing 10 % Col6AA05.

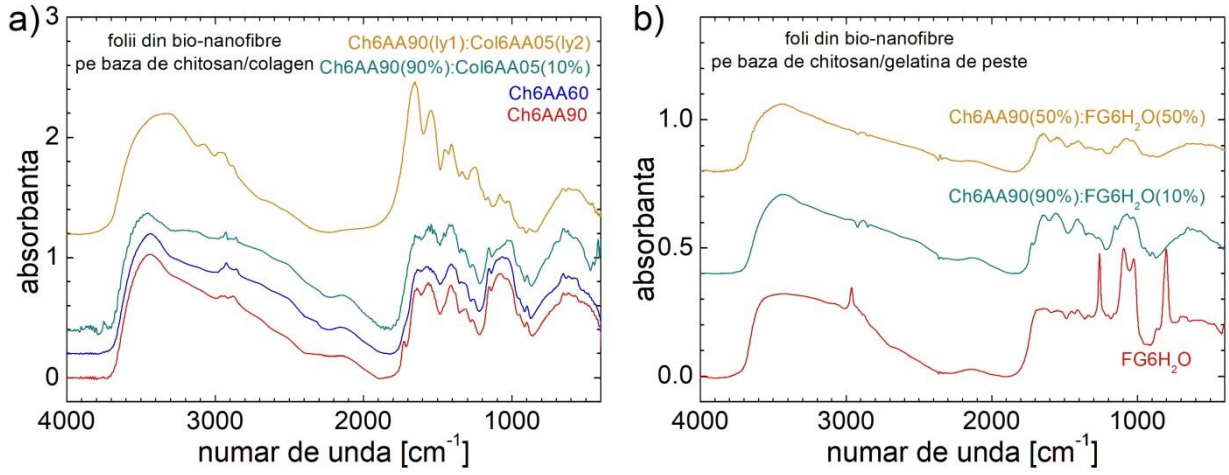

Fig. 8.3. FT-IR spectra of electrospun bio-nanofibre films prepared on the basis of a) collagen and chitosan and b) fish gelatin and chitosan [53].

8.3 Characterization of SEM

One of the classic methods of characterizing nanofibers is performed using scanning electron microscopy (SEM). The resolution at different magnifications of SEM images is more than adequate for the structural characterization of nanofibers obtained by electrospinning. The geometric arrangement and effect of chitosan for bio-nanofiber electrospun films is best indicated by SEM images. These images are shown in Fig. 8.4 for samples Ch6AA60(90%):Col6AA05(10%) and FG6H2O.

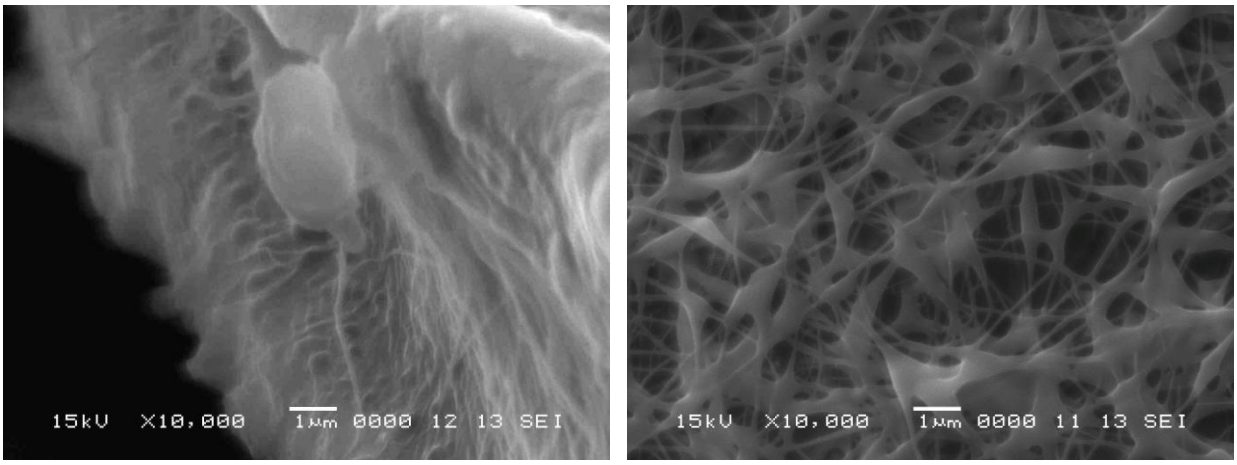

Fig. 8.4. Scanning electron microscopy (SEM) images of bio-nanofibre films (a) Ch6AA60(90%)Col6AA05(10%) and b) FG6H2O obtained by electrospinning [53].

The use of chitosan, as a major component of electrospun bio-nanofibers, leads to the formation of a densely packed film consisting of successively deposited layers, while the last layer of nanofibers is deposited on the last surface and merges significantly with the existing biomaterial (see Fig. 8.4a).

a) FG6H2O

b) PVA6AA90

c) PEG6AA90

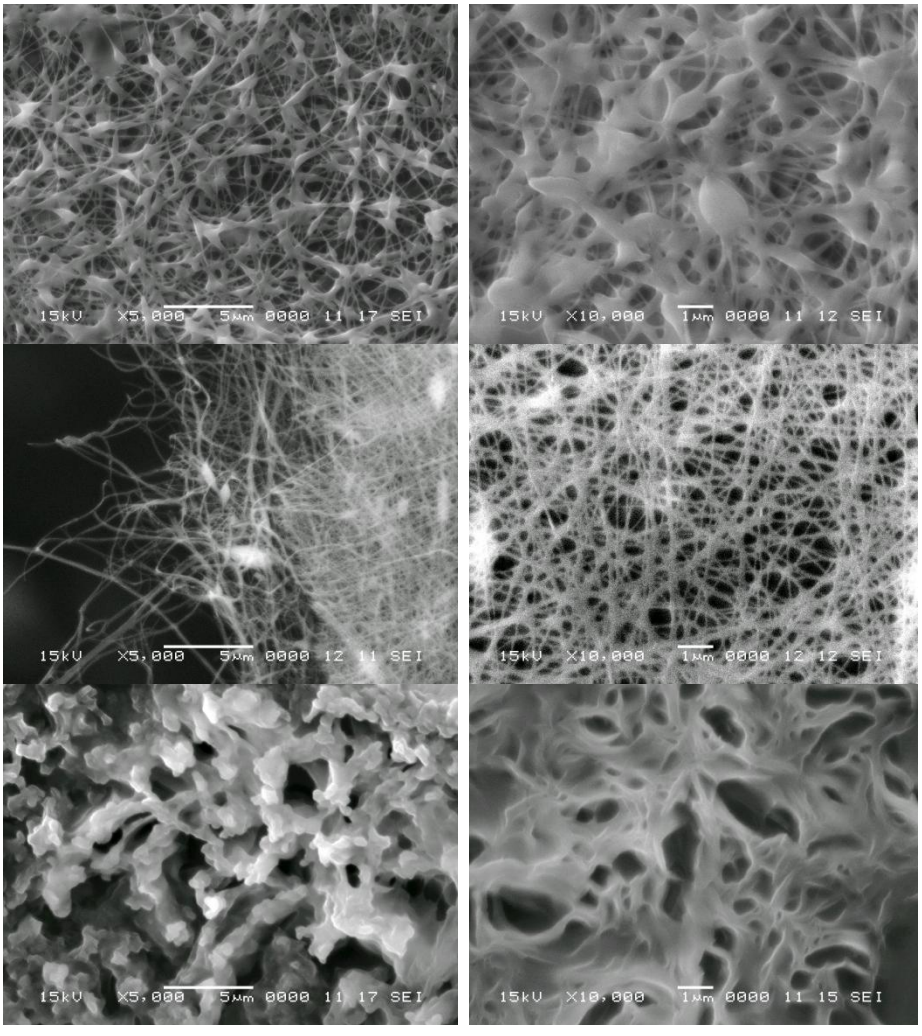

d) Ch6AA90(50%)FG6H$_2$O(50%)

e) Ch6AA90(90%)PVA6AA90(10%)

f) Ch6AA90(50%)PEG6AA90(50%)

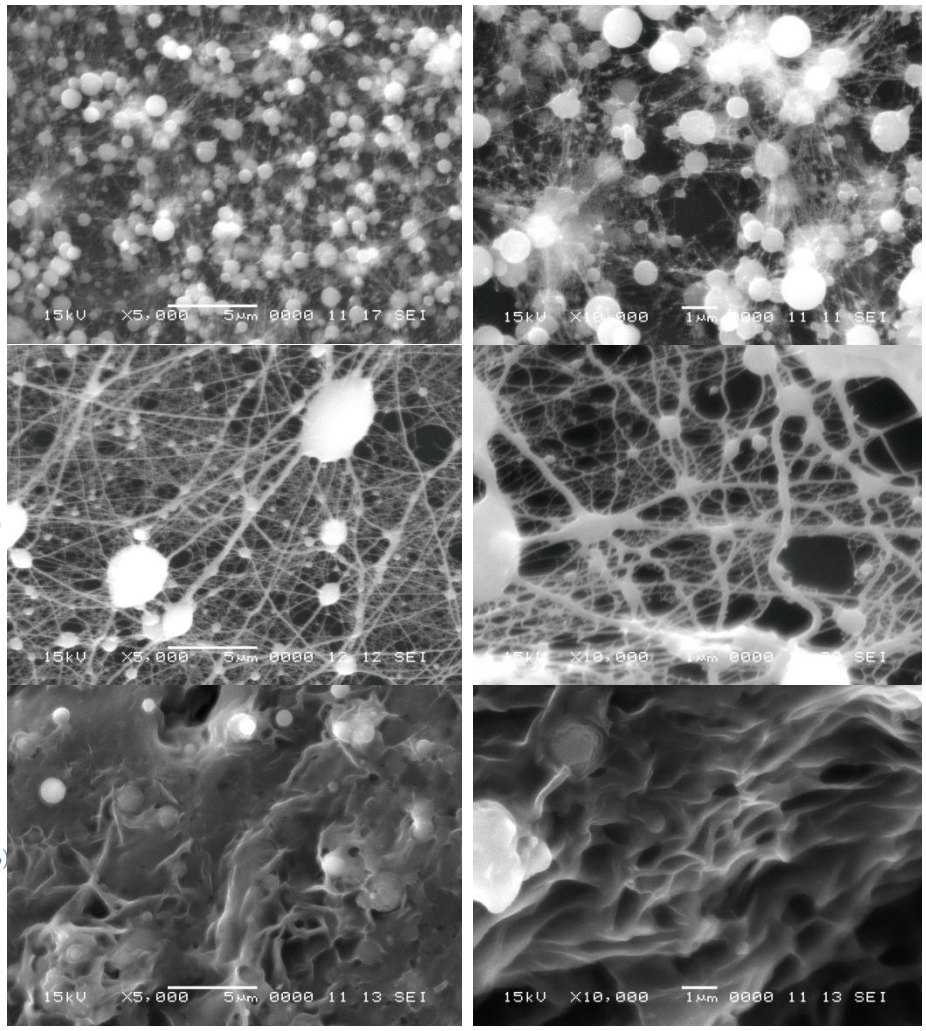

Fig.8.5. Scanning electron microscopy (SEM) images with magnification of ×5000 (left) and ×10000 (right) measured for bio-nanofibre films a) FG6H2O; (b) PVA6AA90; (c) PEG6AA90; d) Ch6AA90(50%)FG6H2O(50%); e) Ch6AA90(90%)PVA6AA90(10%); f) Ch6AA90(50%) PEG6AA90(50%) [59].

The main fibers can be considered to form a so-called mesh network. Secondary fibers with a diameter of half (½) to one-tenth (~1/10) of the diameter of the primary fibers form a local secondary network. They are characterized by a length of less than 1 μm to a few micrometers and are usually connected directly to the primary network, but can also be connected through *small bulbs*. Several tertiary fibers can form another local network and join the secondary fibers through direct bonds. A tertiary fiber can join two secondary fibers without further contact, but other tertiary fibers can be seen showing cross-linking nodes in a small number. At this magnification of the SEM images, the quaternary fibers (of the fourth order) are difficult to be observed.

CHAPTER 9 ARTIFICIAL NEURAL NETWORKS USED FOR THE CHARACTERIZATION OF NANOFIBERS PRODUCED BY ELECTROSPINNING

9.1 Characterization of the degree of local order of nanofibers using artificial neural networks

The analysis-prediction procedure was applied on some of the measured SEM images. First it was observed that the predicted order is not a unique value and can best be described as an interval. This is a reasonable approach for nanofibers with so many characteristics other than linear fibers (see the previous discussion related to the characterization of SEM images). Thus, it can be seen that the single-component nanofiber film based on fish gelatin FG_6H_2O has a degree of order in the range of 0.287 – 0.472. This means that the fibers are mostly disordered. The most disordered nanofibers were found for the two-component Ch6AA90(50%):FG_6H_2O(50%) film produced from fish gelatin. The predicted degree of order was in the range of 0.051 – 0.312, which placed these networks as being made up of almost totally disordered nanofibers. The degree of density of the nanofiber network can also play an important role in the analysis of the degree of order, as can be seen from the set of two images shown in Figure 9.1 (third row) for the two-component Ch6AA90(90%):PVA6AA90(10%) foil. As expected, a denser network can be characterized by a more heterogeneous fiber orientation, with a degree of nanofiber ordering in the range of 0.281 – 0.520. Here it can be seen that some parts of the nanofiber network have crossed the boundary from disordered to ordinate of 0.5. A less dense network has a narrower range of order (0.157 – 0.368) and can generally be characterized as more disordered than a dense network. The last two sets of predictions (last row in Fig. 9.3) obtained for PVA-based films, two-component nanofiber films Ch6AA90(90%) PVA6AA90(10%) and single-component PVA6AA90 show that the degree of clutter can increase with the increase in the number of components.

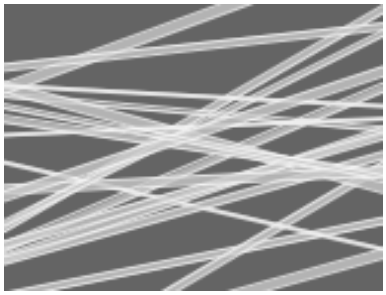

The predicted degree of order (0.380)

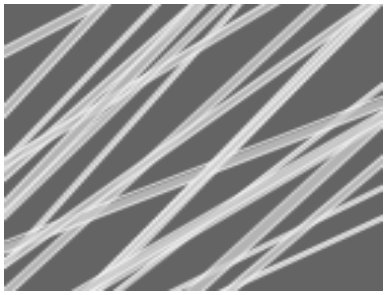

The predicted degree of order (0.618)

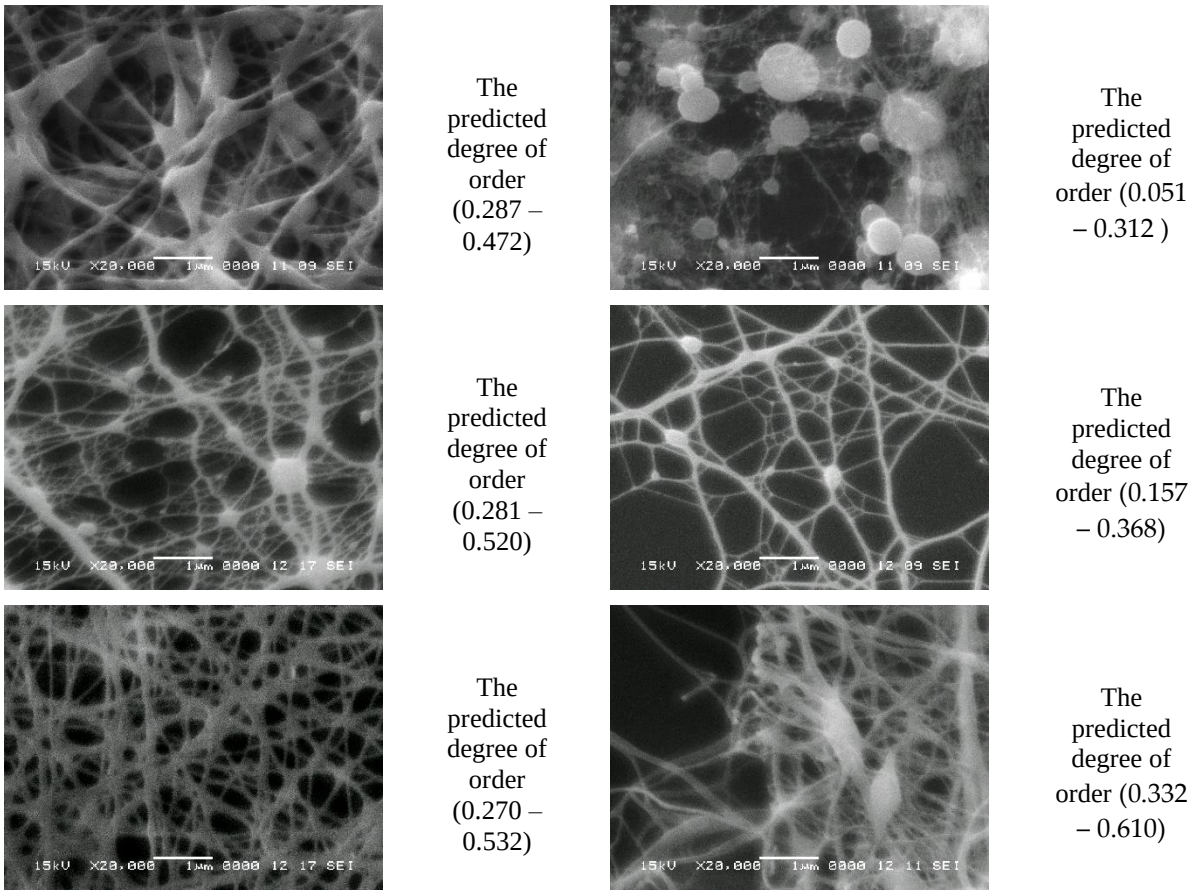

Fig. 9.1. ANN-predicted degree of electrospun nanofibers from simulated fiber images with a) 0.33 and b) 0.66 degrees of order and from SEM images measured at a magnification of ×20000 for foils c) FG6H_2O; d) Ch6AA90(50%)FG6H_2O(50%); e) and f) Ch6AA90(90%)PVA6AA90(10%); g) and h) PVA6AA90 [59].

9.2 Principal Component Statistical Analysis and Use of Artificial Neural Networks

Principal Component Analysis (PCA) is a powerful tool for assessing the statistical behavior of measured data, allowing the discrimination of different parts of a statistical system, finding correlations between different types of parameters and, where appropriate, observing a process of evolution. The main result of applying the PCA analysis to measurements involving biosolids (as described in Chapter 3 biosolids-based organo-mineral fertilizers) of sludge and wastewater from a poultry slaughterhouse is shown in Fig. 9.4 as a graph of PC2 (second main component) as a function of PC1 (first main component) [62]. Here, the contributions of each parameter (total absorbance of the VIS-IRnear spectra, $T_{2,1}$ spin-spin relaxation time, self-diffusion coefficient D_1, pH, EC and TDS) are considered as the weight with which the main components from PC1 to PC6 are calculated. In order to assess the importance of a particular parameter for each main component, only the quantities of the listed values should be taken into account.

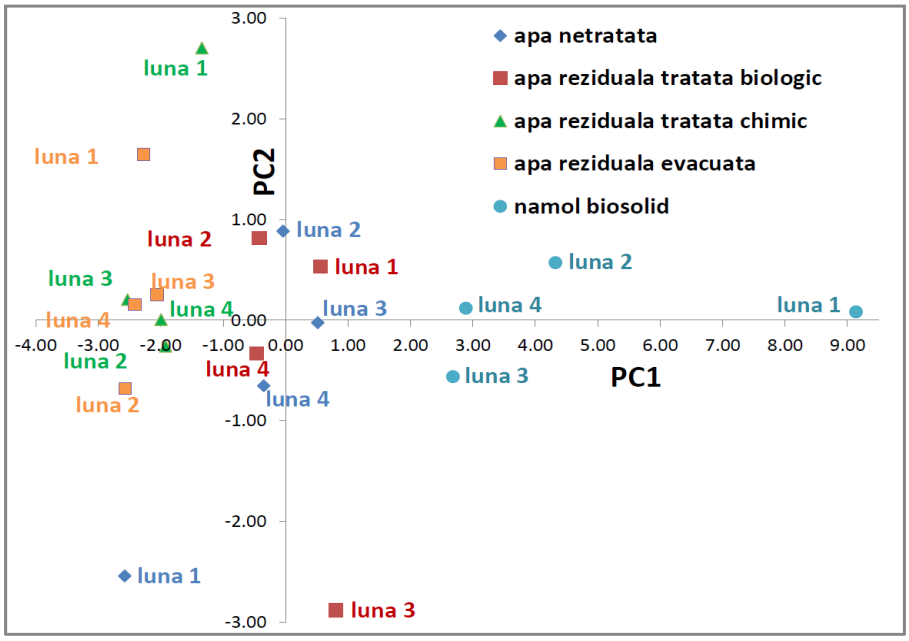

Fig.9.2. PCA: Statistical analysis in principal components: 2D graph of the function PC1 versus PC2 obtained for wastewater (untreated, biologically treated, chemically treated and discharged) and samples of biosolid sludge used as fertilizer collected in four months of monitoringe [62].

The sign of the enumerated values will contribute to the displacement of the data presented in Fig. 9.2 and will lead to the separation between different types (groups) of samples. The first main component FP1 is characterized by the highest data separation, and the displacement (variation) decreases with the increase in the number of the main component, thus PC6 has the smallest displacement. In Figure 9.2, the group of four points (from month one to four monitoring) corresponding to untreated wastewater which are shown in blue diamond. For months 2, 3 and 4 these points are located in the center of the figure with the lowest values of PC1 and PC2. The point corresponding to month one of monitoring untreated wastewater is located at a high negative of PC1 and PC2. Some contribution can be found to come from the NMR parameter, $T_{2,1}$ (-0.561). The lowest contribution to PC1 comes from pH (0.25) and total absorbance measured in VIS-IRnear (0.336). In contrast, the main contribution to main component 2 (PC2) comes from pH (0.794). Also, the total absorbance in the near VIS-IR (-0.627) can also be credited with a large contribution. At FP2 an insignificant contribution comes from $T_{2,1}$ (0.054), and then from TDS (0.165) and EC (0.22). The NMR self-diffusion coefficient, D_1 will have a relatively important contribution (0.343). Therefore, the pH, EC and TDS measurements taken for the samples collected in the first month of monitoring are outside the expected range. A similar behavior can be found for wastewater and biologically treated water (the square filled with red in Fig. 9.2). Here, the points corresponding to the samples collected in months 1, 2 and 4 are grouped, and the point corresponding to month 3 is largely shifted in the negative direction of FP2. Therefore, the pH

value and total absorbance in near-IR-VIS measured for this sample are primarily responsible for this out-of-group position.

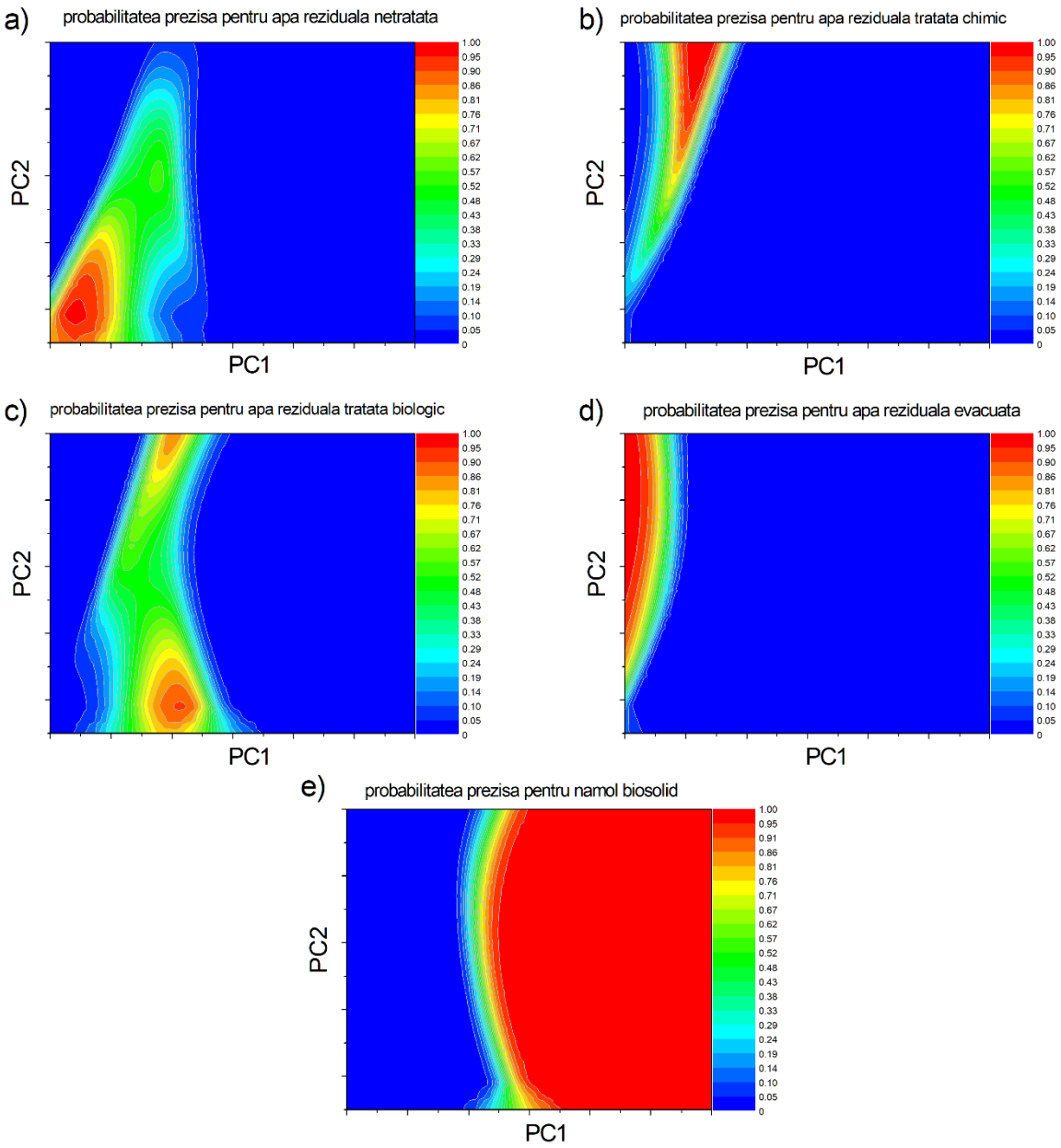

Fig.9.3. Predicted probability using ANR for (a) untreated wastewater, (b) chemically treated wastewater, (c) biologically treated wastewater, (d) discharged wastewater, and (e) biosolid sludge [62].

FINAL CONCLUSIONS

1. A research plan was developed that was used for complex characterization using advanced methods, of biomaterials such as nanofibers obtained by electrospinning and biosolids used as organo-mineral fertilizers.

2. An electrospinning device used for the production of mono- and two-component nanofiber films by electrospinning, based on chitosan, collagen, fish gelatin, PVA and PEG has been successfully designed, built and tested.

3. In collaboration with the National Institute for Research and Development for Machinery and Installations for Agriculture and Food Industry-INMA Bucharest- Cluj-Napoca Branch, 3 types of biosolids used as organo-mineral fertilizers were obtained by extrusion.

4. The ^{1}H NMR relaxometry was successfully used for the complex characterization of organo-mineral fertilizers, raw materials used for electrospinning, precursor solutions and nanofiber films.

5. The two-dimensional NMR relaxometry of the T_2-T_2 EXSY and T_1-T_2 COSY types was used for the first time to characterize the molecular exchange processes and dynamic components of the bio-nanofibers produced within the experimental program of this thesis.

6. Localized high-field NMR spectroscopy has been successfully used to study the distortion of collagen dissolved in acetic acid solutions according to its concentration.

7. NMR spectroscopy measurements were performed in high fields of ^{1}H and ^{13}C below MAS for the 3 types of organo-mineral fertilizers and subtle changes due to minor variations in their components were highlighted.

8. FT-IR spectroscopy has proven to be a successfully used method for the complex characterization of both organo-mineral fertilizers and raw materials used for electrospinning, precursor solutions and finally nanofiber films.

9. X-ray diffraction has been successfully used for the structural characterization of raw materials used for electrospinning as well as biosolids used as organo-mineral fertilizers.

10. Scanning electron micrograph (SEM) confirmed the production of nanofibers with complex morphology (shape, structure, size and connectivity) strongly influenced by the type and concentration of the biomaterials used. In addition, coupled with EDX it proved to be essential for the clarification of the component elements, newly formed by extrusion and obtaining biosolids used as organo-mineral fertilizers.

11. It was shown that classical measurements, used to determine the physicochemical parameters of some solutions, such as pH, electrical conductivity and TDS, turbidity, refractive index and viscosity, can also be used intelligently. In this regard, dynamic pH and electrical conductivity measurements were used to determine the amount of fertilizer released, a specific release time and a rate of release of fertilizers in distilled water solutions.

12. The data analysis was complex and involved several levels, starting from the primary processing of the measured data, continuing with their analysis involving the 1D Fourier transform and the 1D and 2D Laplace transform, the deconvolution of the Laplace and Fourier spectra, the quantitative analysis and ending with the statistical principal component analysis (PCA) enhanced by the use of artificial intelligence that involved the use of artificial neural networks and machine learning.

BIBLIOGRAPHY

1. S. Dharadhar and A. Majumdar, "Biomaterials and Its Medical Applications", Application of Biomedical Engineering in Neuroscience, 355-380, 2019, doi: 10.1007/978-981-13-7142-4_18.
2. A. Bharadwaj, "An overview on biomaterials and its applications in medical science", *in IOP conference series: materials science and engineering, IOP Publishing, 2021, April*, Vol. 1116, No. 1, p. 012178.
3. Y.C. Ahn, S.K. Park, G. T. Kim, Y. J. Hwang, C.G. Lee, H.S. Shin, et al, "Development of high efficiency nanofilters made of nanofibers", Curr Appl Phys, 6:1030–5, 2006.
4. J. Zeleny, "The electrical discharge from liquid points, and a hydrostatic method of measuring the electric intensity at their surfaces", Phys Rev 3:69–91, 1914.
5. G.I. Taylor, "Electrically Driven Jets", Proc R Soc Lond, A Math Phys Sci, (1934–;313, 453-75, 1990.
6. S.Y. Chew, Y. Wen, Dzenis Y, Leong KW. The role of electrospinning in the emerging field of nanomedicine. Curr Pharm Des, 12:4751–70, 2006.
7. D. Liang, B.S. Hsiao, B Chu, "Functional electrospun nanofibrous scaffolds for biomedical applications", Adv Drug Deliv Rev 59:1392–412, 2007
8. A.L. Yarin, S. Koombhongse, D.H. Reneker, "Bending instability in electrospinning of nanofibers", J Appl Phys., 89:3018–26, 2001
9. S Ramakrishna, K Fujihara, W.E. Teo, T. Yong, Z. Ma, R. Ramaseshan, "Electrospun nanofibers: solving global issues", Mater Today, 9:40–50, 2006.
10. L.A. Smith, P.X. Ma, "Nano-fibrous scaffolds for tissue engineering", Colloid Surf B, 39: 125–31, 2004.
11. N. Bhardwaj, S. C Kundu, "Electrospinning: A fascinating fiber fabrication technique. Biotechnology advances, 28(3), 325-347, 2010.
12. N. Cioica, C. Coța, E. M. Nagy, Z.Gyorgy, C. Nicola, "Reactive Extrusion Processing of Nutrient-Enriched Biosolids", INTERNATIONAL SYMPOSIUM, INMA TECH 2020.
13. C. Coța, N. Cioica, E. M. Nagy, Z. Gyorgy, , R. Fechete, "Research Regarding the Realisation of Granular Organo-Mineral Fertilizers Based on Biosolids", INTERNATIONAL SYMPOSIUM, INMA TECH, 2019.
14. H. Kominko et al., "Sustainable Management of Sewage Sludge for the Production of Organo-Mineral Fertilizers", Waste Biomass Valorization, vol. 9, pp. 1817–1826, 2018.

15. V. Kumar et al., “A review on sewage sludge (Biosolids) a resource for sustainable agriculture”, Archives of Agriculture and Environmental Science, vol. 2, no.4, pp. 340-347, 2017.
16. R. Pöykiö, G. Watkins, O. Dahl, ”Characterisation of municipal sewage sludge as a soil improver and a fertilizer product”, Ecological Chemistry and Engineering S, vol. 26, no. 3, pp.547-557, 2019.
17. H. Kominko et al., ”The Possibility of Organo-Mineral Fertilizer Production from Sewage Sludge”, Waste Biomass Valorization, vol.8, pp. 1781–1791, 2017.
18. H. Kominko et al., ”Closing the nutrient cycle by using organo-mineral fertilizers based on secondary raw material”, Proceedings of 7th International Conference on Sustainable Solid Waste Management, Heraklion, Greece, pp. 1-15, 2019.
19. E. M. Nagy et al, ”Research on the realization of biocomposite ecofertilizing granular materials based on peat”, Annals of the University of Craiova -- Agriculture, Montanology, Cadastre Series, vol.. XLVIII/2018, pp.344-349, 2018.
20. .
21. M. Warne, M. McLaughlin, D. Heemsbergen, M. Bell, K. Broos, M. Whatmuff, G. Barry, D. Nash, D. Pritchard, D.Stevens, G. Pu, *Draft Position Paper recommendations of the Australian National Biosolids Research Program on Biosolids Guidelines*, 2008.
22. D.L. Pritchard, N. Penney, M.J. McLaughlin, H. Rigby, K. Schwarz, ”Land application of sewage sludge (biosolids) în Australia: risks to the environment and food crops”, Water Sci. Technol. 62 (1), 48–57. 2020
23. **R.Crainic**, E. M. Nagy, G. Fodorean, M. Vasilescu, P. Pascuta, F. Popa and R. Fechete, “Advanced NMR, FT-IR, VIS-nearIR and XRD methods used for characterization of organo-mineral fertilizers based on biosolids”, Agriculture 14, 2024.
24. B.M.M.N. Borges, D.B. Abdala, M.F. de Souza, L.M. Viglio, M.J.A. Coelho, P.S. Pavinato, and H.C.J. Franco, “Organomineral phosphate fertilizer from sugarcane byproduct and its effects on soil phosphorus availability and sugarcane yield”, Geoderma 339, 20–30 (2019).
25. C. Lu and H. Tian, “Global nitrogen and phosphorus fertilizer use for agriculture production in the past half century: Shifted hot spots and nutrient imbalance”, Earth Syst. Sci. Data 9, 181–192 (2017).
26. A.E. Johnston, D. Curtin, and K. Syers, Efficiency of Soil and Fertilizer Phosphorus Use, FAO: Roma, Italy, 2008.

27. M. Pawlett, L.K. Deeks, and R. Sakrabani, “Nutrient potential of biosolids and urea derived organo-mineral fertilizers in a field scale experiment using ryegrass (Lolium perenne L.)”, Field Crops Res. 175, 56–63 (2015).

28. M.C. Paré, S.E. Allaire, L.É. Parent, and L. Khiari, “Variation in the physical properties of organo-mineral fertilisers with proportion of solid pig slurry compost”, Biosystems Engineering 106(3), 243–249 (2010).

29. L.K. Deeks, K. Chaney, C. Murray, R. Sakrabani, S. Gedara, M.S. Le, ... and G.H. Smith, “A new sludge-derived organo-mineral fertilizer gives similar crop yields as conventional fertilizers”, Agronomy for Sustainable Development 33, 539–549 (2013).

30. R. Fechete, D. E. Demco, D.C. Moldovan, R.I. Chelcea, E. Culea, “Rezonanța Magnetică Nucleară, Metode Clasice și Moderne, Ed. Risoprint” Cluj-Napoca, 2010.

31. J. Keeler, Understanding NMR Spectroscopy, 2nd ed., John Wiley & Sons, Ltd, Chichester, West Sussex, United Kingdom, 2012.

32. L. Venkataramanan, Y.Q. Song, and M.D. Hürlimann, “Solving Fredholm integrals of the first kind with tensor product structure in 2 and 2.5 dimensions”, IEEE Transactions on Signal Processing 50, 1017–1026, 2002.

33. M.D. Hürlimann, S. Utsuzawa, and C.Y. Hou, “Spin dynamics of the Carr-Purcell-Meiboom-Gill sequence in time-dependent magnetic fields”, Phys. Rev. Appl. 12, 044061, 2019. https://doi.org/10.1103/PhysRevApplied.12.044061

34. C. Duan, C. Ryan, S. Utsuzawa, Y.Q. Song, and M.D. Hürlimann, “Effect of off-resonance on T1 saturation recovery measurement in inhomogeneous fields”, J. Magn. Reson. 281, 31–43, 2017. https://doi.org/10.1016/j.jmr.2017.05.003

35. Y.Q. Song, Y. Tang, M.D. Hürlimann, and D.G. Cory, “Real-time optimization of nuclear magnetic resonance experiments”, J. Magn. Reson. 289, 72–78, 2018. https://doi.org/10.1016/j.jmr.2018.02.009

36. Y.Q. Song, “Magnetic Resonance of Porous Media (MRPM): a perspective”, J. Magn. Reson. 229, 12–24, 2013. https://doi.org/10.1016/j.jmr.2012.11.010

37. Smith, Brian C. Fundamentals of Fourier transform infrared spectroscopy. CRC press, 2011.

38. Brian C. Smith, Infrared Spectral Interpretation: A Systematic Approach. CRC Press, Boca Raton, 1999.

39. Brian C. Smith, Quantitative Spectroscopy: Theory and Practice. Academic Press, San Diego, 2002.

40. S. Bourne, A. Haefner, K. Norton, and P. Griffiths, Anal. Chem. 62: 2448, 1990.

41. P. Griffiths and J. DeHaseth, Fourier Transform Infrared Spectrometry, 2nd ed., Wiley, New York, 2007.

42. M. Diem, P. Griffiths, and J. Chalmers, Eds., Vibrational Spectroscopy for Medical Diagnosis, Wiley, New York, 2008.

43. C.A. De Caro and C. Haller, UV/VIS Spectrophotometry—Fundamentals and Applications, Mettler-Toledo International, 2015.

44. Y. Waseda, E. Matsubara, and K. Shinoda, X-ray Diffraction Crystallography: Introduction, Examples and Solved Problems, Springer Science & Business Media, 2011.

45. W. Zhou, R. Apkarian, Z.L. Wang, and D. Joy, "Fundamentals of scanning electron microscopy (SEM)", Scanning Microscopy for Nanotechnology: Techniques and Applications, 1–40, 2007.

46. C. Lu and H. Tian, "Global nitrogen and phosphorus fertilizer use for agriculture production in the past half century: shifted hot spots and nutrient imbalance", *Earth Syst. Sci. Data* 9, 181–192, 2017.

47. FAO. Efficiency of Soil and Fertilizer Phosphorus Use. 2008.

48. C. Borgia, R.J.S. Brown, and P. Fantazzini, "Uniform-Penalty Inversion of Multiexponential Decay Data", J. Magn. Reson. 132, 65–77, 1998.

49. I. Lacan, M. Moldovan, and I. Ardelean, "The Influence of Chitosan on Water Absorption and Solubility of Calcium Phosphate Cement", Coatings 13, 1641, 2023. https://doi.org/10.3390/coatings13091641.

50. Z. Movasaghi, S. Rehman, and I. U. Rehman, "Fourier Transform Infrared (FT-IR) Spectroscopy of Biological Tissues", Applied Spectroscopy Reviews, 43(2), 134–179, 2008.

51. **R. Crainic,** A.S. Farcașanu, P. Păscuță, L.D. Șaitiș, F. Popa, R. Fechete, "Complex characterization of nanofibers biomaterials based on chitosan, collagen and fish gelatine produced by electrospinning", Analytical Letters, S. 1-29, 2024, doi: 10.1080/00032719.2024.2372348.

52. S. Kataki, S. Hazarika, and D. C. Baruah, "Investigation on by-products of bioenergy systems (anaerobic digestion and gasification) as potential crop nutrients using FTIR,

XRD, SEM analysis and phyto-toxicity test", Journal of Environmental Management, 196, 201–216, 2017.

53. M. Dhawan, R. Sharma, and G. Sharma, "EDX and X-Ray Technique in Forensic Science", in Advances in Analytical Techniques for Forensic Investigation, 339–362, 2024.

54. R. F. Melo-Silveira, G. P. Fidelis, M. S. S. P. Costa, C. B. S. Telles, N. Dantas-Santos, S. O. Elias, V. B. Ribeiro, A. L. Barth, A. J. Macedo, E. L. Leite et al., "In Vitro Antioxidant, Anticoagulant and Antimicrobial Activity and Inhibition of Cancer Cell Proliferation by Xylan Extracted from Corn Cobs", International Journal of Molecular Sciences, 13, 409–426, 2012.

55. W. F. Wolkers, A. E. Oliver, F. Tablina, J. H. Crowe, "A Fourier-transform infrared spectroscopy study of sugar glasses", Carbohydrate Research, 339, 1077–1085, 2004.

56. F. R. F. Silva, C. M. P. G. Dore, C. T. Marques, M. S. Nascimento, N. M. B. Benevides, H. A. O. Rocha, S. F. Chavante, E. L. Leite, "Anticoagulant activity, paw edema and pleurisy induced by carrageenan: Action of major types of commercial carrageenans", Carbohydrate Polymers, 79, 26–33, 2021.

57. M. Todica, L. Udrescu, Experimental Methods in Polymer Physics, Presa Universitară Clujeană, Cluj-Napoca, Romania, 2013.

58. **R. Crainic**, L. R. Drăgan, R. Fechete, "Structural investigations of polymer-based materials", Studia Universitatis Babeș-Bolyai, Physica, 63, 49-60, 2018.

59. **R. Crainic**, P. Păscuță, F. Popa, R. Fechete, "NMR, FT-IR, XRD, SEM and ANN characterization of nanofibers materials produced by electrospinning", Materials, (in preparation, 2024).

60. R. Fechete, D.E. Demco, X. Zhu, W. Tillmann, and M. Möller, "Water states and dynamics in perfluorinated ionomer membranes by 1H one-and two-dimensional NMR spectroscopy, relaxometry, and diffusometry", Chemical Physics Letters 597, 6–15, 2014.

61. R. Fechete, D. Moldovan, and R. Chelcea, Applications of Modern NMR Techniques to Nanocomposite Materials and Biomaterials, ISBN: 978-973-662-906-8, Editura U.T. PRESS, Cluj-Napoca, 2013.

62. **R. Crainic**, R. Fechete, "Slaughterhouse Wastewater Properties Assessment by Modern and Classic Methods", Water, 16, 2382, 2024. DOI: 10.3390/w16172382.

LIST OF PUBLICATIONS IN THE FIELD OF THE THESIS

Papers published in ISI journals

1. R. Fechete, I.A. Morar, D. Moldovan, R.I. Chelcea, **R. Crainic**, S.C. Nicoara, Fourier and Laplace-like low-field NMR spectroscopy: The perspectives of multivariate and artificial neural networks analyses, *Journal of Magnetic Resonance* 324, 106915, (2021) (IF: 2.516, AIS: 0.68).
2. **Ramona Crainic**, A. S.Farcașanu, P. Pășcuță, L. R. Șaitiș, F. Popa, Radu Fechete, Complex Characterization of Nanofiber Biomaterials Based on Chitosan, Collagen and Fish Gelatine Produced by Electrospinning." *Analytical Letters* (2024): 1-29 (IF: 1.6, AIS: 0.267).
3. **Ramona Crainic**, Radu Fechete, Slaughterhouse Wastewater Properties Assessment by Modern and Classic Methods. *Water* 2024, 16, 2382. https://doi.org/10.3390/w16172382 (IF: 3.0, AIS: 0.529).
4. **Ramona Crainic**, E.M. Nagy, E.M.; Fodorean, G.; Vasilescu, M.; Pascuta, P.; Popa, F.; Fechete, R. Advanced Nuclear Magnetic Resonance, Fourier Transform–Infrared, Visible-NearInfrared and X-ray Diffraction Methods Used for Characterization of Organo-Mineral Fertilizers Based on Biosolids. *Agriculture* 2024, 14, 1826. https://doi.org/10.3390/agriculture14101826 (IF: 3.3, AIS: 0.469).
5. **Ramona Crainic**, Petru Pășcuță, Florin Popa and Radu Fechete, NMR, FT-IR, XRD, SEM and ANN characterization of nanofibers materials produced by electrospinning, Materials, (in preparation 2025).

Papers presented at international conferences

1. **Ramona Crainic**, E. M. Nagy, N. Cioica, and R Fechete, 1H NMR relaxometry and FT-IR spectroscopy used for characterization of organo-mineral fertilizers based on biosolids, ^{13}th biennial International Conference on Processes in Isotopes and Molecules PIM-INCDTIM, 22-24 September 2021, Cluj-Napoca, Romania.

2. **Ramona Crainic**, Alexandru Stefan Farcasanu, Petru Pascuta, Lavinia Raluca Saitis, and Radu Fechete, Advanced experimental and numeric simulation method used for the characterization of nanofibers biomaterials produced by electrospinning. ^{33}th Anual Conference of the European Society for Biomateriales ESB2023, 4-8 September 2023, Davos, Switzeland.
3. **Ramona Crainic**, A Fărcăsanu, P Păscută, L R Saitis and R Fechete, Experimental and numeric simulation used for the characterization of nanofibers biomaterials produced by electrospinning, ^{14}th biennial International Conference on Processes in Isotopes and Molecules PIM-INCDTIM, 19-22 September 2023, Cluj-Napoca, Romania.